A NEURO-INSPIRED OCULOMOTOR CONTROLLER FOR A ROBOTIC HEAD PROTOTYPE

BY PRAVEENRAM BALACHANDAR

A thesis submitted to the

Graduate School—New Brunswick

Rutgers, The State University of New Jersey

in partial fulfillment of the requirements

for the degree of

Master of Science

Graduate Program in Computer Science

Written under the direction of

Prof. Konstantinos P. Michmizos

and approved by

_____

_____

_____

New Brunswick, New Jersey

May, 2017

ABSTRACT OF THE THESIS

A Neuro-inspired Oculomotor Controller for a Robotic Head Prototype

by Praveenram Balachandar

Thesis Director: Prof. Konstantinos P. Michmizos

Robotic vision introduces requirements for real-time processing of fast-varying, noisy information in a continuously changing environment. In a real-world environment, convenient assumptions, such as static camera systems and deep learning algorithms devouring high volumes of ideally slightly-varying data, are hard to survive. Leveraging on recent neural studies that show smooth pursuit - that is the slow movement of the eyes - and saccade - their rapid movement - being handled by the same neuronal circuitry, we designed a neuromorphic oculomotor controller and placed it at the heart of a biomimetic robotic head prototype that we designed and built. The oculomotor controller is unique in the sense that 1) the encoding and processing of information is done via spikes communicated across models of biological neurons, and 2) it mimics the brain structure and therefore requires no training to operate. Interestingly, the tracking performance of our proposed system is comparable to that of PID controllers while the robotic eye kinematics are strikingly similar to those reported in human eye studies. This work contributes to the overarching goal of ComBra Lab, which is to develop neuro-mimetic "bottom-up" computational models of brain networks, where the emerged intelligence is used to control robots.

Acknowledgements

Journeys in the body of science and technology are never solo travels. The droplet of water this thesis signifies in the ocean of science is no exception. In addition to the shoulders of giants that I've built my work upon, I'd like to thank Aditya Vinjamuri, for his help with neuroscience throughout the thesis, in helping me find research articles and to better understand the neurological basis of vision and oculomotor control. I'd also like to thank Leo Kozachkov, for his help in modeling the coordination between conjugate and vergence movements. I'd also like to thank other members of ComBra lab for assisting in subtle ways throughout the process, through their own work and their presentations. Last, but definitely the most important, I'd like to thank Prof. Konstantinos P. Michmizos for guiding me through this thesis, from identifying a problem statement to helping me perfect the spiking neural network model for the robot prototype. Most of all, I'd like to thank him for his motivation and belief in my work.

As human beings we rely on social interactions to flourish in our lives. It is only fair that we acknowledge those who've helped us keep our sanity as we tread the waters of science. First and foremost, I'd like to thank my parents, K. Balachandar and Chitra Balachandar, for supporting me financially and otherwise in this distant land away from home. I'd also like to thank my friends, for the endless, sometimes pointless, debates and conversations that helped me focus whenever I was at work.

Dedication

To my parents and family,

for always believing in me and pushing my limits.

To Manali,

for inspiring me to be a better version of myself.

To friends,

for being there and getting me back on track whenever I drifted.

To scientists,

decades of whose efforts have laid the foundation for my work.

Table of Contents

List of Figures

Chapter 1

Introduction

The brain is considered as the final frontier of knowledge. Since 1700 BC, the first recorded reference to the brain (1), the study of brain function and dysfunction has evolved from being philosophical, to a behavioral approach and finally, to a quantitative approach. Over the last century, advancements in brain imaging techniques (95) and ability to record single cell firing patterns (96) have allowed us to study the function and dysfunction of the brain at a neuronal level. However, the fact remains that we don't entirely understand how the brain works yet.

Even with the limited understanding we have today, neuroscience has furthered the evolution of robotic systems. Humanoid robots, an emergent area in robotics, and robots in general, were previously designed only as tools (97) and operated purely on rationality without room for emotion (98). Computer scientists have been trying to build sentient beings embodied with emotion using conventional methods but the challenges with these techniques are insurmountable (99). To the contrary, the humanoid robot iCub (2), developed by the Italian Institute of Technology, deviates from this conventional approach and mimics key processes in the mammalian brain as its control system (100). This approach has enabled the iCub to learn in the same way an infant does, by performing small actions and learning from their consequences. Since its introduction in 2008, has learnt several new skills including archery (101), solving 3D puzzles and displaying emotion through facial expressions. We take inspiration from works such as these in our efforts to build a neuro-mimetic spiking neural network for the oculomotor system.

Spiking neural networks (SNNs) evolved from Artificial neural networks (ANNs).

In a categorization of neural networks by Mass (1997, 1998), the first generation neural networks had computational units which represented only binary state, like the multilayer perceptrons (102), Hopfield networks (103) and Boltmann machines (104). The second generation that followed had neurons that were more biologically plausible, which supported continuous input and output such as the saturation neuron and sigmoidal neuron (105). The second generation neuronal networks are commonly used in many machine learning applications today (106). The third generation, spiking neural networks (SNNs), were more biologically accurate in that they communicated only through spikes. The neurons respond to excitatory and inhibitory input spikes by changing their internal state, similar to the fluctuation in membrane potential of a real neuron, generating an output spike only when conditions favorable for generating an action potential are met. The SNNs encode and understand information encoded by timing of the spikes (107) as well as the presence (or absence) of spikes, which makes them particularly suited for spatio-temporal pattern tasks (108). Although the SNNs can do everything the previous generation of ANNs could do, the only challenge with SNNs is that there are no guidelines for designing functional SNNs.

The neuro-mimetic SNN we propose, handles this challenge by imitating structure found in the brain and using biologically constrained learning rules to train the network. Conventional learning approaches in neural networks such as backpropagation or gradient descent cannot be applied to SNNs because of the asynchronous and sparse response of the neurons, therefore there is no differentiable signal and we're forced to use techniques such as imitating structure and using biologically constrained learning rules to build functional SNNs. In this thesis, in addition to building a functional oculomotor controlled based on SNNs, we also show that by imitating the control structures observed in the brain, behavior is automatically built into the system even without learning.

In this thesis, conducted at the Computational Brain (ComBra) Lab at Center for Computational Biomedicine Imaging and Modeling (CBIM), Rutgers University under the guidance of Prof. Konstantinos P. Michmizos, we've built a biomimetic robotic head controlled by a spiking neural network. The SNN has been designed to process

a visual stimulus, provided by a laser pointer, and track it in real-time by generating oculomotor saccade commands using a neuro-mimetic spiking neural network.

The remainder of this report is organized as follows. In chapter 2, we discuss the hardware components used to build the robot head and the control mechanism used to interface the robot with the computer which will act as the brain for the robot. In chapter 3, we discuss the neural basis of vision. We introduce how the eyes interpret our surroundings and how an image is represented in the brain. In chapter 4, we discuss the different types of eye movements and the distinction in their control from a neural perspective. In chapter 5, we describe in detail, control of saccades by the oculomotor system and introduce our model. In chapter 6, we present results. Finally, in chapter 7, we present future work and discussion.

Chapter 2

Hardware Design

Bio-mimetic factors drove the design of the prototype robotic head. We analyze the human visual system for factors such as field of view of each eye, range of movement of each eye, as well as the range of movement of the neck. These factors determine the extent of the visual field from a stationary position in a room. Each eye has a 210 (150) degree field of vision horizontally (vertically), though most of the peripheral vision is blurred (3). To shift focus to these blurry areas, each eye is equipped with the ability to move 100 (70) degrees horizontally (vertically). In addition, we have the ability to move our neck with 3 degrees of freedom (DOF), which are termed flexion, extension, lateral rotation and lateral flexion. For simplicity, we restrict the movement of the neck to only flexion, extension, lateral rotation and ignore lateral flexion, hence restricting it to 2 DOF.

The above design features 6 degrees of freedom (DOF). This includes 2 DOF for the neck and 2 DOF for each eye. Each 2 DOF sub-system is designed as a pan/tilt mechanism to allow for horizontal and vertical movement from a fixed point. If this design were to be compared to the human system, it accounts for the extra-ocular muscles and the vestibular muscles of the neck. The eyeball is an intricate system of muscles that help in focusing the object on the retina (screen of the eye). We're ignoring the focusing abilities of the eye for this prototype and relying on autofocus capabilities of the camera in its place.

When dealing with custom hardware, accuracy and consistency are two important aspects that need to well understood and documented. To that end, calibration is as important as the experiment itself. For our experiments, we had to calibrate the movement of the robot for various target positions in the test environment. Since we

have used standard non-linear calibration techniques, the process of calibration and the results obtained have been documented as part of the Appendix A.

In the following sections, we describe each of the components that went into building the prototype.

2.1 Pan / Tilt Sub-system:

The pan/tilt system is at the core of our system. Two servos are required to support two degrees of freedom (DOF). This system allows for a range of vertical and horizontal positions. To understand how the system works and its range of motion, we'll describe the individual components of the system and how they are attached together to form the overall system.

2.1.1 Servo

The servo is the active component of the pan/tilt system. It can be visualized as the equivalent of muscles. By organizing the servos in different configurations, human like movement can be emulated. Although it is a versatile component, the internal structure is rather simple. It consists of a motor and circuitry to control the exact position of the rotor shaft (of the motor).

There are different types of servos depending on their resolution, torque, speed, range of movement, and power rating.

Torque is a measure of the rotational force. It is inversely proportional to the speed of rotation of the motor shaft. It determines the ability of the servo to maintain a specific position when there is an opposing force in the opposite direction, including against gravity. As a direct correlation, it determines the accuracy with which the servo can hold each position within its range of operation.

Resolution is related to accuracy but it is also a measure of the smallest change in the position of the servo. Indirectly, it is a measure of the reliability and consistency of the servo.

Speed is the measure of the rotation rate of the servo. Given a 360 degree range

of motion around the motor shaft, speed is the number of degrees that the servo can move in a specific direction in a defined time period. When the shaft rotates, the torque reduces and the torque increases only when the motor shaft is at its final desired position.

Range of movement is the number of degrees of motion around the motor shaft (out of 360) that is allowed by the servo. In most hobby servos, the range of motion is restricted to 180 degrees. There are some servos which allow continuous rotation, i.e. 360 degrees of unrestricted motion.

Power rating of a servo is a measure of the amount of power the servo consumes during operation. This is an important factor when the robot needs to run on battery power and is mobile. However, for our prototype we consider that the robot will be plugged in to AC power throughout the duration of operation, so this is not a deciding factor.

Another distinction in servos is based on their mode of operation: analog and digital. Analog servos operate based on alternating on/off voltage signals in a pulse width modulated (PWM) input signal. This can have a maximum of 50 pulses per second. However, digital servos have a microprocessor to receive input and translate it into a pulse train at the rate of 300 pulses per second thereby providing consistent torque and quicker, smoother responses. Although they consume more power they are worth it in advanced robotics applications.

Based on the above parameters, for our prototype we have chosen digital servos which have high torque, high resolution, moderate speed and 360 degree range of movement.

We've used Dynamixel AX-12A digital servos for our prototype. They are the preferred servos for many humanoid and hexapod robot structures produced by Bioloid. The added benefit of using Dynamixel servos is that they are programmable, i.e. they can be programmed to replicate different sequence of positions for different inputs. However, we will not be using this feature in our prototype. They can also be daisy chained and hence the number of servo ports required on the controller is reduced.

The specifications of the Dynamixel AX-12A servo are shown in Table 2.1. Each

Property	Value
Torque	$15.3kg - cm$
Speed	$0.169sec/60\deg$
Power	$10.8W$
Operating Angle	$300\deg$
Resolution	$0.29\deg$

Figure 2.1: Dynamixel AX-12A Servo. Table 2.1: Specifications: Dynamixel AX-12A Adapted from Trossen Robotics.

Dynamixel Servo has a unique numeric value, called ID, which can be configured. The programmed positions / postures of the robot are fed to each individual servo based on their unique ID. Although we do not use the programmable feature of the servos, we use the IDs to change the position of the servo.

The range of positions of the servo are represented as values between 0 - 1023. To move a servo to a new position, a command with the unique ID of the servo and the new position value between 0 - 1023 is sent to the servo.

It is also worth mentioning that the Dynamixel servos interact using the Serial (TTL) interface for communication between one another and with the central controller. In our prototype, we use an Arbotix-M Robocontroller as the central controller. However, the Spiking Neural Network running on a computer generates the commands for the individual servo positions. These commands are sent to the central controller using a serial (USB) connection. The central controller in turn sends the command to each of the servos.

2.1.2 Assembly / Design

As was mentioned earlier, the pan/tilt system requires for the servos to be placed one on top of the other. The steps followed to assemble each of the three pan/tilt components of the prototype were as follows:

- One of the AX-12A servos is fixed to a board which makes the base of the pan/tilt system.

- A metallic bracket is fixed on top of the servo's rotor head. We'll call this the

pan bracket (F3), as seen in Figure 2.2 (b).

- The second servo is fixed upright on the bracket.

- A different tilt bracket (F2) is fixed on top of the second servo providing an elevated platform parallel to the floor / base of the system, as seen in Figure 2.2 (a).

- Any component that needs to have 2 DOF is then fixed on top of this elevated platform.

These metallic components which tie the different parts together and provide structure are equivalent to the skeletal system in the humans. Together with the servos, they form the musculoskeletal system of the robot.
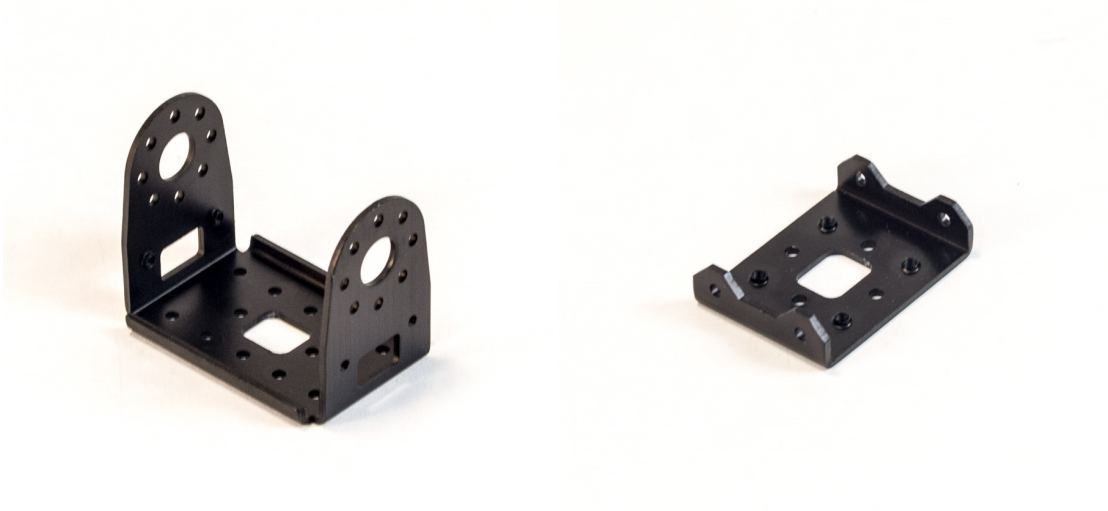
Figure 2.2: Left: F2 Bracket - For Tilt mechanism of the eye. Right: F3 Bracket - For pan mechanism of the eye. Adapted from Trossen Robotics.

The next core component of the prototype is the central controller, which is an Arbotix-M Robocontroller.

2.2 Arbotix-M Robocontroller

The central controller acts as an interface between the computer, which runs the spiking neural network (SNN), and the servos which act as the equivalent of the muscles in

humans.

The Arbotix-M robocontroller is an arduino compatible robot controller. It is designed specifically to be an advanced control solution for Dynamixel / Bioloid actuators and servos. Arbotix-M is a smaller version of the Arbotix controller but with the same capabilities as a controller albeit with fewer ports.

Being Arduino compatible, the programming interface is similar to the Arduino programming interface, i.e. the Arduino IDE. It is also compatible with the wide range of libraries that come with the arduino ecosystem.

The Arbotix-M has a powerful microcontroller, ATMEGA644p, capable of controlling more than 20 Dynamixel servos at a time through the TTL interface. The board is directly compatible with the Dynamixel AX-12A servo. It has 3 TTL ports for Dynamixel servos onboard. Multiple servos can be daisy chained using only these 3 ports. In our prototype, we'll be using the Arbotix-M to daisy chain 6 Dynamixel AX-12A servos.

In addition to controlling the servos, the Arbotix-M is also used to power these servos. It can be powered with an external AC adapter. Depending on the number of servos, different power supplies with a voltage rating of 12V and varying power ratings are used. For our system, the 12V 10A power supply is used with the Arbotix-M to power the 6 servos that will be part of the system. To handle the load, the Arbotix-M also features dual motor drivers.

The Arbotix-M is shown below in Figure 2.3. In this system, it will be used with the FTDI to USB interface to connect to the PC for programming and sending commands from the SNN to the servos. It also supports a XBEE Wireless interface which operates on the same hardware serial port.

2.3 Camera

The last core component of the system is the camera. There are a wide variety of cameras available, but for stereo vision we need to keep in mind a few parameters while choosing the camera. The important points to look for are, global shutter, resolution,
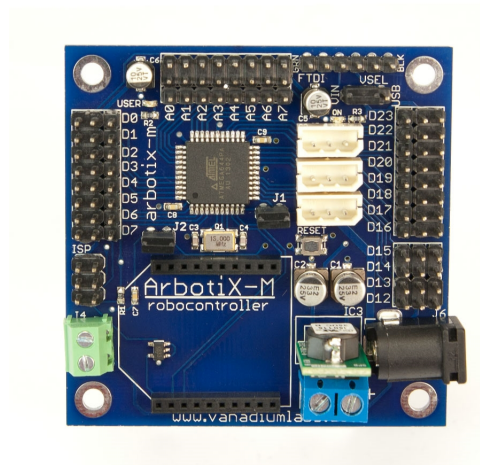
Figure 2.3: Arbotix-M - Arduino Compatible Dynamixel Servo Controller. Adapted from Trossen Robotics.

frame rate and interface.

Global Shutter

The idea behind global shutter is to make sure all the pixels of a frame are captured at the same instant of time. Most web cameras have this feature since they are used primarily for video recording which requires a global shutter or in most cases no shutter at all.

Resolution

Most cameras have at least a resolution of 640x480. This is good enough for most stereo vision systems. The higher the resolution, the more processing power is needed to process the video feed in real time.

Frame Rate

The frame rate is a key aspect for video processing. At higher frame rate, smaller movements can be captured. The concept of frame rate for the human eye doesn't make sense since there is no refreshing of the state of the eye (retina), but instead the eye continuously processes the visual information. Purely based on the maximum rate of change that can be perceived, the frame rate for a human eye is estimated to be

between 60 - 120 fps. Typical webcams do not provide such a high frame rate, and are limited to around 30 fps. Higher frame rate implies more processing as well and the bottle neck shifts to the algorithm used for processing the video feed.

Interface

The interface is crucial part to make sure the system can work together in tandem. Typically, cameras have USB interface. It works best with PCs and is the most preferred choice. The choice of interface should ensure that the frames recorded by the camera can be quickly transmitted the PC for processing in real time.

Auto Focus

Auto focus is an added advantage in some web cameras. If the object is too close or too far, a typical camera with fixed adjustable focus will need lot of manual intervention to fix the camera focus. Auto focus make it easier for the camera to adjust to some changes that can be expected in the real world environment.

Based on the above considerations, we have picked the Microsoft LifeCam Cinema Webcam. It features 720p video at 30 fps and has auto focus capabilities. The camera is mounted on top of the pan / tilt system to make an eye of the robot. In our model, the frames from the camera are resized to a square format with a resolution of 720x720.

Figure 2.4: Microsoft LifeCam Cinema Webcam. Adapted from Trossen Robotics.

2.4   Laser

The laser is the target for the robot. It is mounted on an independent pan/tilt system controlled by a regular Arduino board. This pan/tilt system uses standard hobby servos which lacks the accuracy and resolution of the Dynamixel AX-12A. However, the laser is a gross target and errors in position are acceptable. To obtain more accurate results, a possible future refinement is to use digital servos such as the Dynamixel AX-12A.

The laser is incident on a wall in front of the robot and controlled by an independent program running either on the same computer running the SNN or any other computer. The whole laser system is lightweight and can also be moved manually to generate a randomly moving target for the system.

In the future, an additional laser target will be introduced such that, there are differences in the characteristics of motion of the two targets. This would promote the SNN to select a salient target to follow.

2.5   Interfacing with the computer

An important aspect that makes the hardware functional is the programming of the Arbotix-M controller which is the interface between the SNN and the servos. Being based on the Arduino platform, we used the Arduino IDE v1.0.5. The code, written in C, reads servo position information from the serial (TTY) interface and sends the command to the servo. Although simple in terms of logic, the commands were sent as raw bytes over the serial interface without any protocol. This minimized the overhead for communication allowing better real-time response from the robot. However, the messages were sometimes garbled and a primitive protocol had to be implemented. In this prototype, we verify that the robot received the correct command by sending back the message as received by the controller to the PC. The message was sent to the controller from the PC until the correct message was sent back.

The parameters that affected the communication link were the bit rate of the serial link, the polling delay at Arbotix-M and the time between issuing a command to the servos to move and proceeding to the next instruction in the sequence, we'll call this

delay as the servo movement time. For our prototype, we've chosen:

- Bit rate of serial link: 115200 bits per second

- Polling Delay at Arbotix-M: 5 ms

- Servo movement time: 5 - 10 ms

The command from the SNN to the Arbotix-M is a sequence of integer values between 0 - 1023. As an example, the command could be [500, 512, 500, 500, 500, 500]. In our prototype, we've assigned the IDs as follows:

Neck Pan/Tilt: 1 and 2

Left Eye Pan/Tilt: 3 and 4

Right Eye Pan/Tilt: 5 and 6

Hence, assuming a 1-based index for the array of values shown in the example, the values at the index identified by the servo ID are sent to the servo as the new position command.

It should also be noted that all the servos are set to their median / center position (512) at the start of the experiment, i.e. when the SNN is initialized.

The laser pan/tilt system connected to the Arduino is also interfaced through a similar mechanism. However, since it uses primitive servos, the range of motion of those servos is limited to 180 degrees. They are controlled by sending an angle value between 0 - 180 indicating the position for each of the two servos. The bit rate for this link is chosen to be 9600 bits per second.

2.6   Experimental Setup

Overall, the system has two parts, the laser target control system and the prototype robot head. The prototype robot head is assumed to be fixed to a sturdy surface, such that it doesn't move around on the surface due to movement of the eyes or the neck. This is achieved either by using nuts and bolts to screw the base of the robot onto the surface or by using adhesives.

The laser system is assumed to be in front of the robot head, but not connected to the head in any way. This position in front ensures that there are no objects in between the laser and the wall.

The wall is assumed to be flat and for all practical purposes it can be assumed to be of infinite length with respect to the range of the head. The distance between the wall and the robot head prototype is very important for calibration and estimation of the angle between the target and the fovea.

For the results that follow, we've placed the prototype at a distance of 55 cm from the wall where the target is shown. The origin with respect to which all recordings are made is assumed to be at the center between the two eyes and at the height of the fovea of the eyes.

The eyes and neck are also assumed to always start from the initial position where they are all centered with respect to their servo positions, i.e. all the servos are initialized to the position 512. This position is equivalent to staring straight ahead. The setup described above is shown in Figure 2.5.
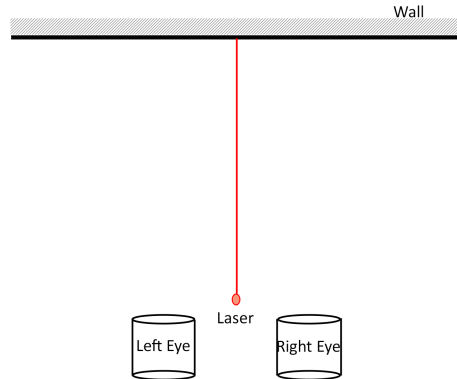
Figure 2.5: Experimental Setup with the two eyes and the laser in between the two eyes in its initial position.

The overall system connection diagram is shown in Figure 2.6.
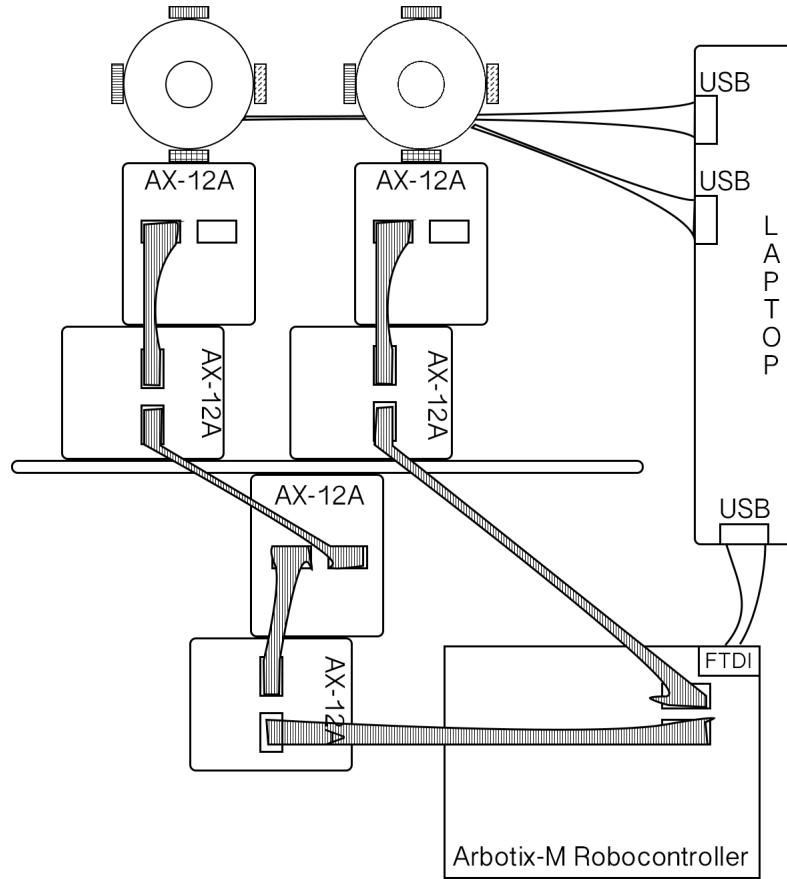
Figure 2.6: System connection diagram showing the connection between the different servos, the connection between the servos and the Arbotix-M robocontroller, and the connection of the cameras and Arbotix-M with the computer running the SNN.

The code to control the servos and some parts of the code that is the SNN is made available in Appendix B.

Chapter 3

Neural Basis of Vision

Human beings and mammals have foveated vision which allows them to analyze a limited portion of their field of view in greater detail while at the same time be aware of large changes in their immediate environment (6). From an evolutionary perspective, this stems from a survival instinct. However, human beings, having an evolutionary advantage over most mammals, have a better visual system including color vision. With the ability to perceive greater detail around the fovea and color perception, vision in low light conditions is not as good as in other mammals, like a cat (7). The major difference arising due to the structure of their visual system starting with the retina.

The neural structures involved in vision are formed in the early stages of embryogenesis. Retina, the sensory equivalent for all visual stimuli, is an extension of the central nervous system and is formed during embryogenesis (8). Unlike the motor system, recent studies indicate that the neural structures that control eye movements based on visual stimuli are well established before birth (9). Although the brain adapts and grows rapidly after birth, these structures do not undergo significant change.

Being the gateway to vision, we'll begin our journey through the visual system at the retina as we briefly discuss the different areas of the brain that are involved in visual processing and their function.

In the rest of the chapter we'll discuss how the retina converts light impulses into action potentials, the pathway in the brain that these action potentials travel through and finally how the brain interprets these action potentials within the context of the oculomotor system.

3.1   Retina

The retina is the first layer of processing in the visual pathway. Light incident on the retina is converted into a series of action potentials that represent information. The action potentials encode simple details like the intensity of the light. They also encode the different patterns and colors observed in the visual field. As we'll see, the process in which these action potentials are generated and the pathways in which they travel are different.

The processing in the retina is predominantly based on the structure and the predefined connections between neurons. Although it is an extensive neural network, there is limited learning from a conventional artificial neural network perspective.

3.1.1   Structure

The retina is a thin membrane composed of different layers of neurons at the back of the eye. At a high level, each layer has a different purpose and the neurons of the layer are specialized for the specific function (4).

An interesting aspect about the structure of the retina is that the functional order of the layers is opposite to the physical ordering of the layers. This structure helps in delivering nutrients to the neurons in the retina through the blood vessels while at the same time also ensuring that there is no noise due to reflection of light from within the eye ball (10).

The main layers of the retina, in their functional sequence are:

- Photoreceptor layer

- Bipolar cell layer

- Ganglion cell layer

The above layers are in a feed-forward neural network structure with limited interaction within the layer. There are also intra-layer and feedback neurons in the retina. These are mainly the horizontal cell layer and the amacrine cells. These neurons form synaptic connections within the layer providing information about a different part of the visual
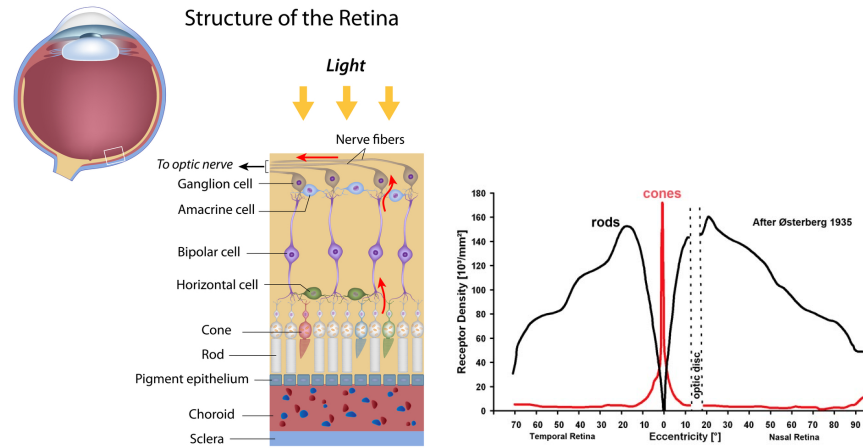
Figure 3.1: Left: Neural layers of the retina. Right: Photoreceptor distribution in the retina around the fovea. Images adapted from Webvision, University of Utah.

field to another neuron thereby helping in pattern recognition (11), contrast, and light intensity equalization (12, 13).

It is well known that there are two types of photoreceptors, mainly the rods and cones. As was mentioned earlier, the human visual system is foveated and supports color vision. This can be observed from the structure of the photoreceptor layer of the retina (14, 15), as can be seen in Figure 3.1 (b).

Cones which are associated with color vision, play a major role in extracting visual detail from our environment. They are found in more concentration around the fovea and the number of cones reduces as we move towards the periphery of the retina.

Rods which are associated with low light vision, play a major role in detecting gross movements and large changes in the visual field. They are found in more concentration towards the periphery of the retina and reduce in number towards the fovea / center of the retina.

As we go down the layers, the bipolar cells have varying dendritic fields. They connect with varying number of photoreceptors depending on the eccentricity from the fovea. The region around the fovea, where cones dominate, there is almost a one-to-one photoreceptor (cone) to bipolar cell ratio (17). As we move towards the periphery the dendritic field grows and the bipolar cells connect with upwards of 40 rods (16).

This specific variation in the dendritic field size accommodates for the variation in

the light sensitivity between the cones and rods. In low light conditions, cumulative response from the rods at the bipolar cells (with wider dendritic fields) enables gross vision sensitive to sudden changes in light intensities. In bright conditions, the cones have the dominant response and the one-to-one bipolar cells near the fovea enable detailed analysis of the objects in the visual field.

In the next layer, we have the ganglion cells. These cells form what are known as the center-surround receptive fields of the eye (18). There are two types of center-surround receptive fields, ON-center, OFF-surround and the OFF-center, ON-surround (19). Like the name suggests, the on and off depend on illumination. However, contrary to what the name suggests, the on and off do not represent complete lack of illumination and presence of light. They represent relative differences in intensity of light or contrast (21). This acts as a mechanism to identify edges / boundaries in the field of view (20). The response of a ON-center, OFF-surround ganglion cell under different illumination profiles is illustrated in Figure 3.2 (b). It is important to note that the ganglion cells innervate primarily with the cone bipolar cells.

These receptive fields are derived from the structure of neurons in the retina. There are two types of bipolar cells, ON and OFF bipolar cells. The ON bipolar cells have longer axons and reach into sublamina **b** of the inner-plexiform layer (IPL) and the OFF bipolar cells with shorter axons only reach into sublamina **a** of the IPL as illustrated in Figure 3.2 (a) (22, 23). In addition to being classified as ON-center and OFF-center, the ganglion cells have two major categories, the Midget (P-type) and Parasol (M-type). The midget ganglion cells are found near the fovea and encode fine detail. The parasol ganglion cells are not sensitive to color and carry more rod related information (24). They are called P-type and M-type because these ganglion cells innervate with the parvocellular and magnocellular regions of the Lateral Geniculate Nucleus (LGN) respectively.
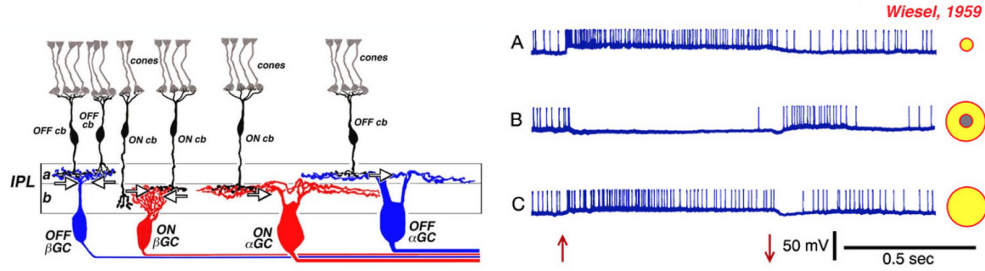
Figure 3.2: Left: Distinction in the innervations from the ON/OFF bipolar cells with the ON/OFF ganglion cells at the Inner Plexiform Layer (IPL). Right: Center Surround response of an ON-center/Off-surround ganglion cell for different illumination. Adapted from Webvision, University of Utah.

The decreasing number of neurons as we go down the layers eventually leads to a photoreceptor to ganglion cell ratio of about 125 to 1.

The other two types of cells, namely the horizontal and amacrine cells are found in the outer plexiform layer (OPL) and inner plexiform layer (IPL) respectively. The horizontal cells have synapses with multiple photoreceptors and bipolar cells across a small region of the visual field. These cells have the crucial role of light intensity equalization or adaptation to sudden brightness changes (25). Due to this property, they also help in forming the center-surround receptive fields. The amacrine cells are involved primarily in the rod pathway. They innervate with rod-bipolar cells in the sublamina **a** of the IPL and in turn form synapses with the cone bipolar cells and the cone ganglion cells providing an indirect pathway for the rod pathway signals (26).

Finally, the ganglion cell axons carrying the visual information is sent through the optic nerve towards the LGN through the optic chiasm where the inputs from the two eyes cross over. The axons are of different diameters with varying conduction velocities (27, 28). The rod signals being simple are the fastest to reach the LGN from the ganglion cells although they take longer time to reach the ganglion cell through the layers of neurons in the retina (29). The cone signals carry a lot of information and are sent through the larger diameter axons in the optic nerve (17). The innervations of the P-type and M-type ganglion cell axons with the different layers of LGN (30) is illustrated in Figure 3.3.
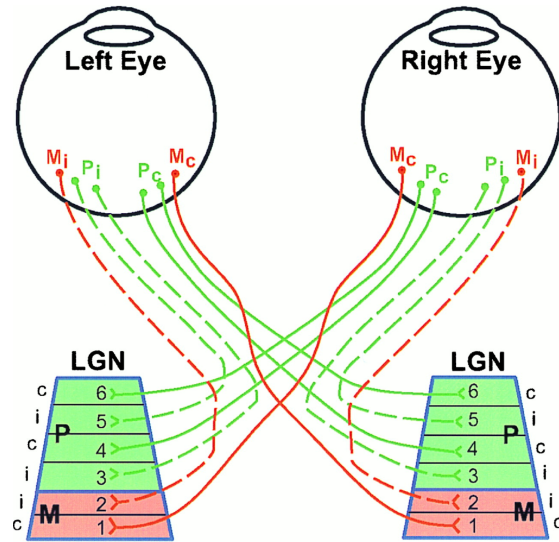
Figure 3.3: P-type and M-type ganglion cell innervations with the different parvocellular and magnocellular layers of the LGN. In this figure, "i" and "c" represent ipsilateral and contralateral, meaning connections from the same side vs connections from the opposite side. Adapted from (109)

3.2 Visual Cortex

The visual cortex is a region of the cerebral cortex in the occipital lobe that deals with processing visual information. The information from the eyes goes through to the LGN and it is sent to the visual cortex from the LGN. In this case the LGN acts like a relay center in the brain. The neurons in different layers of the LGN project to different layers in the primary visual cortex (V1) (4) as shown in Figure 3.4 (a). The visual cortex is further divided into multiple layers V1 to V6 with interconnections between the layers and connections to higher cortical regions of the brain (4). The input from the LGN, which constitutes all the visual input, is sent directly to the V1, which then sends the input to the other layers of the visual cortex as can be seen in Figure 3.4 (b).
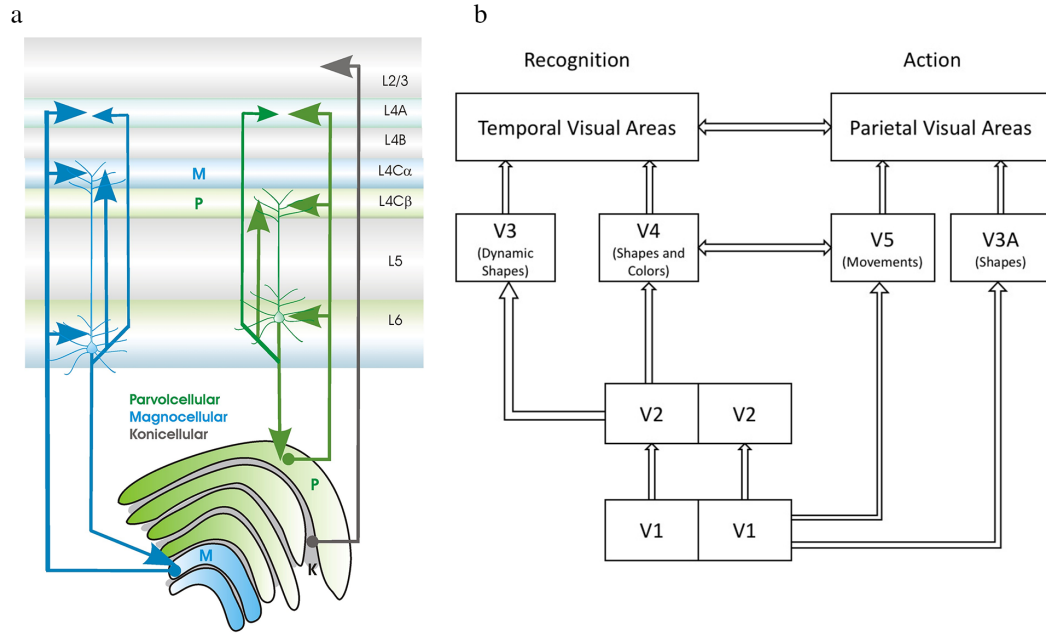
Figure 3.4: (a) Projections from the layers of LGN into the layers of primary visual cortex (V1). Adapted from (110). (b) Interconnections between the layers of the visual cortex (V1 - V6) and the two different visual pathways (where - dorsal and what - ventral).

Each layer of the visual cortex is specialized to process a portion of the visual information. In this section, we'll briefly go over the different function of the layers of the visual cortex (V1 - V6).

3.2.1 Primary Visual Cortex (V1)

The primary visual cortex (V1) is the largest and most important visual cortical area. It receives nearly all the visual input available to the cortex. It is divided into multiple layers and as shown in Figure 3.4 (a), the inputs from the LGN arrive at layer 4 of V1 (32) and the V1 sends back signals to the LGN from layer 6 (31).

As we know, the ganglion cells from the retina innervate with different layers of the LGN. This ganglion cell classification is propagated through into the V1 with different layers within layer 4 receiving inputs from the parvocellular and magnocellular parts of the LGN (33).

As a direct extension, the spatial organization of the ganglion cell within the retina

is also preserved at the V1 based on relative positions of the LGN neurons (34). Within layer 4 of the V1, neurons represent specific regions of the retina from the fovea to the periphery. This retinotopic organization is important in the where pathway to identify where the object is with respect to the fovea / center of the visual field.

In addition to being the first layer of the visual cortex, the V1 has another important function. The V1 has neurons which represent different receptive fields and are selective to specific visual stimuli (35). The receptive fields of the V1 are not circularly symmetric and most are linear. Among the linear receptive fields, there are simple and complex fields (36). The simple fields represent input aligned at specific angles whereas the complex fields represent motion in specific directions as is shown in Figure 3.5. The direction selective neurons in the V1 mainly receive input from the magnocellular pathway and send their response to higher cortical regions specializing in motion related tasks.
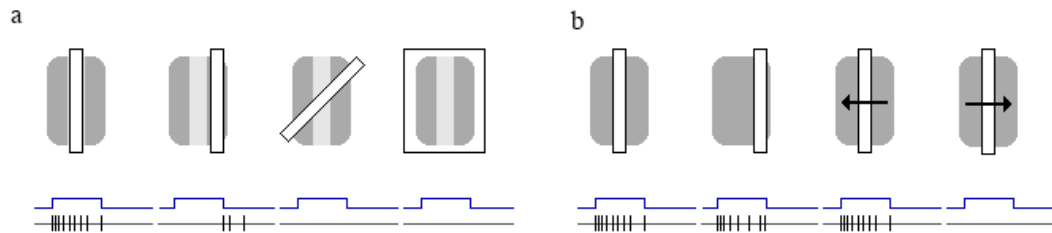
Figure 3.5: (a) Simple Cell receptive field response for stimulus in different angles. (b) Complex cell receptive field response showing direction selectivity for movement of the input.

There are also orientation selective receptive fields in the V1 that use the receptive field representation from the LGN and retina which are both circular symmetric.

Binocular Input / Stereo Vision

In the V1, most of the inputs to the V1 come from the LGN of the same side as the V1. Since there is a crossover of inputs at the optic chiasm before it reaches the LGN, the V1 is the first stage of the visual pathway where binocular input is available. Using the retinotopic organization, the horizontal components of the input are used to deduce

depth information at the V1. This information is represented in the binocular neurons that have different firing rates depending on the depth of the target (37, 38).

3.2.2   V2

The second layer of the visual cortex, it receives most of its inputs from V1 and projects to both the where and what pathways. The neurons of V2 exhibit similar character-istics to those observed in V1 with direction selectivity and receptive fields. The V2 also holds a complete map of the visual world in its dorsal and ventral quadrants in both hemispheres (41). We mention this yet again because propagation of this visual representation through the cortical layers plays a significant role in the oculomotor system.

In recent studies, the V2 has been found to play a role in object recognition memory, visual memory (40), and higher order visual processing like separating background from foreground (39).

3.2.3   V3

The exact function of the third layer of the visual cortex is still under investigation. Anatomically, V3 is split into dorsal and ventral regions (42). Some studies suggest that both the regions have the entire visual map. The dorsal V3 region, as the name suggests, is associated with the dorsal pathway, and is believed to process global motion, i.e. coherent motion of large patterns that cover a major portion of the visual input (43). The receptive fields of the neurons in the V3 are more complex than V1 and V2 and they could represent the presence of specific shapes in the visual input (44).

The portion of the dorsal V3, known as V3A is of interest to us.

3.2.4   V4

The third layer in the ventral pathway, V4 receives its inputs from V2. The V4 layer has neurons that have receptive fields like V2, tuned for orientation, color, and movement. It also has neurons whose receptive fields represent simple objects and shapes (44).

Although, not directly related to the current work, the neurons in V4 also represent selective attention (45) and exhibits plasticity with direct input from the frontal eye fields (FEF) (46). Attention is a higher cortical function and is required for oculomotor responses which involves tracking a specific object in a space of different objects. Hence, the structures in V4 are of interest for future work.

3.2.5   V5 - MT

The V5, also known as the middle temporal visual area has neurons that are highly direction selective. It is known to play an important role in smooth pursuit movements (47, 48). The neurons assist in estimation of direction and speed of movement of an object of interest. These responses are used to match the speed of eye movement with the speed of the object during smooth pursuit. The smooth pursuit movement and the other types of eye movements are discussed in Chapter 4. The structures in this region are also of interest for future work.

3.2.6   V6

The V6, also found on the dorsal pathway, is similar in function to the V5. There are fewer direction selection neurons and the function of the V6 is thought to be related to processing self-motion compared to motion of the object in V5/MT. Hence, the V6 projects to the regions of the brain that control musculoskeletal system and posture and in turn the premotor cortex (49, 50, 51).

The cortical regions highlighted above process the visual information in two distinct pathways and project to higher centers of the brain which make cognitive and motor decisions. One such region is the frontal eye field (FEF) which is involved in oculomotor decisions.

3.3   Frontal Eye Field (FEF)

The frontal eye field is a region in the frontal cortex that contains cells required for preparation and triggering of eye movements. There are other regions associated with

eye movements such as the supplementary eye field (SEF), superior colliculus (SC) and a few other regions of the frontal cortex. The FEF region is of interest to us because it is involved in triggering voluntary saccades and smooth eye movements (pursuit) (52, 53, 54, 55).

Throughout this chapter, we've discussed the concept of a visual map that is represented by a population of neurons at different stages of the visual pathway. The FEF is one such region which contains the visual map (56). It receives its inputs from the other cortical eye fields, some cortical visual regions, higher cognitive centers, and subcortical regions. The FEF projects directly to the pons region of the brainstem (58), known to contain neurons associated with saccades, and to the SC directly and indirectly via the basal ganglia 59. These connections are represented in the Figure 3.6.
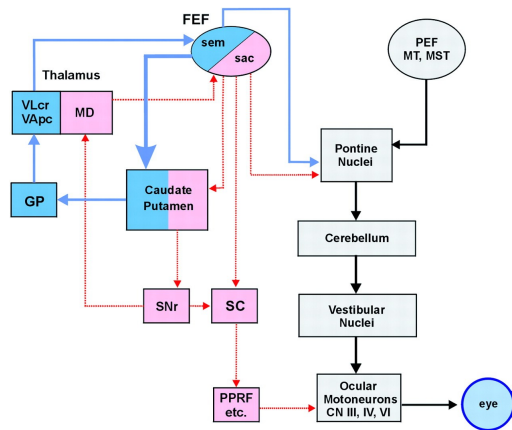
Figure 3.6: The connections illustrating the role of FEF in the generation of saccadic eye movements. Adapted from (111)

The FEF influences the accuracy of eye movements (60, 61). It encodes the visual signals and provides an estimate of the distance towards the target in preparation for eye movements towards the said target. Some cells within the FEF show higher firing rates as the eyes move towards the receptive field of the target, which allows for target selection and better saccade estimation (62).

Saliency Map

The activity of the FEF neurons is equivalent to the generation of a saliency map (56). The initial visual stimulus produces a saccade estimate and depending on the movement towards or away from the receptive field of the intended target, the activity of the FEF neurons adapt to have a peak response around the intended target's spatial location within the FEF. This process involves simultaneous inhibition and excitation of neurons within the FEF. This behavior has been observed even when there is no eye movement, as a continuous process to evaluate the most salient region of the visual map, in preparation for an impending saccade (57).

As shown in Figure 3.6, the FEF projects into the superior colliculus, which we discuss next.

3.4   Superior Colliculus (SC)

The activity of the superior colliculus has a causal effect on saccades, smooth eye movements and neck movements in response to large saccades (64). It is a region in the midbrain that receives inputs from all the sensory systems responsible for generating responses to different sensory inputs and the environment, the central nucleus for coordinating sensory motor transformations (63).

The superior colliculus has several layers and some of these layers are known to have a topographic map of the sensory system they receive input from. The SC layer associated with visual system has a retinotopic map based on the input from the retina and the visual cortex. Encompassing neurons that correspond to both sensory and motor functions, the SC triggers motor commands for sensory input with low latencies (65, 68).

In addition to triggering saccades and pursuit movements, the SC is also involved in maintaining gaze. Fixation neurons found in the rostral SC cause micro-saccades that help maintain gaze around a chosen target (66, 67). The neurons involved in this process might get their input indirectly from the FEF through the basal ganglia since fixation is a conscious action.
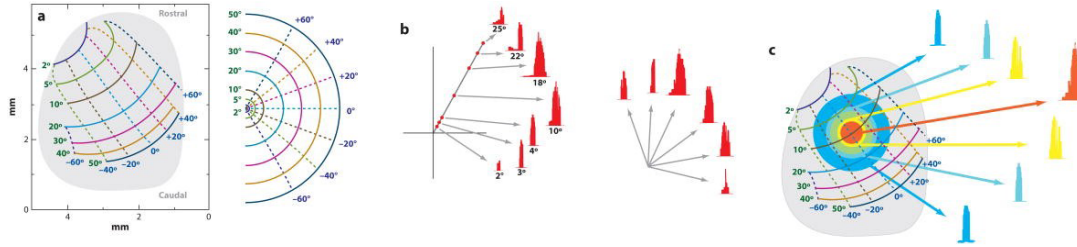
Figure 3.7: (a) A schematic of the topographic organization of contralateral saccade vectors (left) is encoded in retinotopic coordinates. Isoradial and isodirectional bands are shown as solid and dashed lines, respectively. The radial and directions bands are identified in green and blue numbers, respectively. (b) Burst profiles for different amplitude saccades in the optimal direction (left) and for several optimal amplitude saccades in various directions (right). (c) Population response for the generation of a saccade showing suboptimal activity around the neuron that encodes optimal saccade direction. Adapted from (112).

Based on the retinotopic map, the SC neurons evoke a population response that generates both the saccade vector and the kinematics for the movement (68). The response characteristics for the neurons of SC however doesn't vary. The weights of the connections between the SC neurons and the saccade burst generation neurons increases logarithmically from the fovea to the periphery, based on the location of the SC neuron in the retinotopic map (65). The SC responses depending on the retinotopic coordinates is shown in Figure 3.7.

Chapter 4

Eye Movements

The human eye has 6 muscles around the eye ball to move the eye in the orbital socket. This allows movement in both horizontal and vertical directions for each eye. In addition to eye movements, changes in the position of the neck extends the range of vision. The neck movements involve more (larger) muscles to be activated and are invoked only when the eye movement is not sufficient to focus the target on the fovea. In this chapter, we'll look at the different types of eye movements and briefly look at the structure of the eye with a focus on the extra-ocular muscles which control eye movements.

There are 4 basic types of eye movements and the neuronal circuitry involved in the control of these are different. The one common neuronal pathway is the pons region of the midbrain which contains the oculo-motor neurons and the burst generation neurons (69). These neurons get their inputs from different higher cognitive centers depending on the nature of eye movement required. But, the neurons of the pons region of the brainstem generate the response that encodes the direction and amplitude of movement for all movement types.

The different types of movements are saccades, smooth pursuit (smooth eye movements), vergence and vestibulo-ocular movements.

4.1 Saccades

Saccades are rapid, sudden movements of the eyes that abruptly change the point of fixation. The amplitude of saccades can be small (micro-saccades) to very large depending on the position of the target in the visual field. Micro-saccades are usually observed during fixation and are involuntary (71). The larger movements can be both

voluntary and involuntary like reflex actions (72, 73, 74). Large amplitude saccades are observed when gazing around a new environment identifying the different objects or while analyzing the layout of a room.

After a target is presented, it takes 50-150 ms for the saccade to begin (75). In this time, the neuronal circuitry behind saccades computes the position of the target with respect to the fovea and the error signal is converted into activation signals for the extra-ocular muscles to move the eye appropriately. The nature of saccadic eye movement for a stationary target is shown in Figure 4.1. Once a saccade has been initiated it will terminate at its intended position, the direction or amplitude of the saccade cannot be altered mid-flight. However, to compensate for random fast moving targets, turn-around saccades are performed mid-flight to reach the target (76).
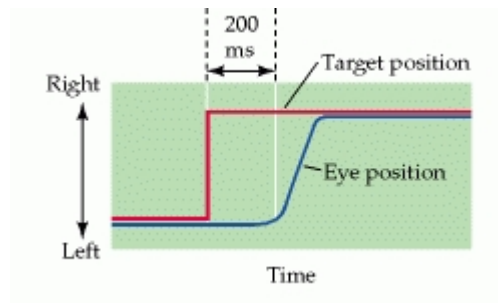
Figure 4.1: Saccade profile for a stationary target towards the right of the visual field, adapted from (70).

The saccadic eye movements are a key part of our prototype and we'll discuss the neuronal circuitry involved in generating saccadic eye movements in the next chapter where we also present our model, spiking neural network.

4.2   Smooth Pursuit Movements

Smooth pursuit movements or smooth eye movements are much slower eye movements designed to keep a moving target on the fovea. It is a voluntary movement and involves several cognitive regions of the brain including a conscious decision making process to follow the target (77). In the absence of a target, smooth pursuit movement relies on trajectory estimation based on previous knowledge of target movement trajectories

(78). In that sense, smooth pursuit relies on real-time trajectory estimation, velocity estimation and association with known target trajectories to issue the final oculomotor command. This phenomenon is observed when the moving target disappears behind an opaque surface, like a wall, to reappear on the other side.

In pursuit movements, there is an initial delay before the target velocity and eye velocity are synchronized. During this time, while estimating the target velocity (79) the eyes are stationary and when the start to move a corrective-saccade is required to focus the target on the fovea (80). After the corrective-saccade the target is kept in the fovea using smooth pursuit movement. This phenomenon is illustrated in Figure 4.2.
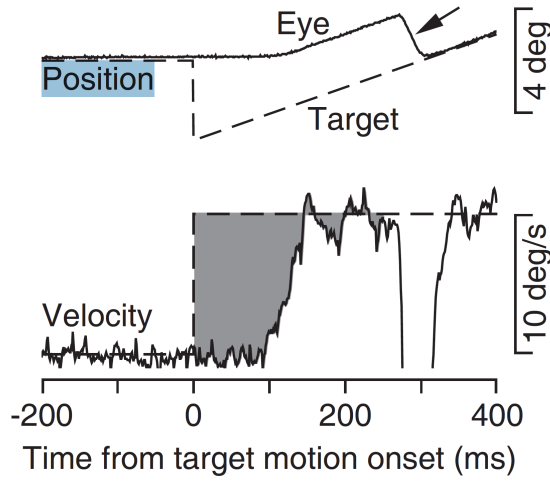
Figure 4.2: Pursuit profile for a target moving at a steady speed. Adapted from (113).

Although we haven't implemented the smooth eye movement in our prototype, the smooth eye movements and saccades share some of the neural structures (69). A future direction of work is to include the structures required for velocity estimation and trajectory recognition into the existing spiking neural network.

4.3 Vergence Movements

The above two types of movements are conjugate eye movements where the eyes move together by the same angle to focus the target on their respective fovea. This is sufficient when the target is far enough from the observer that the angle between the target and

the eye is roughly 0 degrees for both eyes. However, in most real-life scenarios the target is at different angles from the fovea for the left and right eye. An example of such a case is when the target is close to the face. In this scenario, the eyes move towards each other, i.e. both the eyes move medially (towards the nose).

Vergence movements facilitate such dis-conjugate movements of the eyes. They can either converge medially or diverge laterally to accommodate targets near and far respectively. They alternate between convergence and divergence when the target moves closer to and further away from the observer.

In our prototype, we also support vergence movements to accommodate for targets at varying distances from the robot head.

4.4   Vestibulo-ocular movements

The final type of eye movement is exhibited when the head or body is not stationery. When the eyes are fixated on a target and there is a change in the posture of the observer, vestibulo-ocular movements compensate for the posture change while maintaining focus on the target. They are involuntary reflex responses that are driven by sensory information from the semicircular canals of the inner ear (4). In the absence of visual stimuli, the vestibulo-ocular reflex is active only for a short duration of time, after which the eyes return to the neutral position. The reflex is observed only during rapid sudden changes in posture / head position. The other eye movements compensate to focus the eye on the target during slow changes in posture.

A future direction of work is to include vestibulo-ocular reflex in the prototype.

4.5   Extra-ocular muscles

The eye ball is moved around in the orbital socket using the extra-ocular muscles. Like we mentioned at the beginning of the chapter, there are 6 extraocular muscles attached to each eye. These muscles are shown in Figure 4.3.

The muscles that control horizontal movements are the lateral and medial rectus muscles. The inferior and superior rectus muscles, and the inferior and superior oblique

muscles work together to control the vertical movement of the eyes. The oblique muscles also provide torsional force to rotate the eye within the socket (4).

The nuclei that innervate with these muscles are different and the muscles receive the appropriate conjugate or dis-conjugate inputs to move the eyes towards the intended target. The ipsilateral abducens nucleus innervates with the lateral rectus (LR) muscle. The oculomotor neurons from the cranial region VI innervates with the medial rectus (MR), inferior rectus (IR), superior rectus (SR) and inferior oblique (IO) muscles of each eye. Finally, the trochlear nucleus innervates with the superior oblique (SO) muscle.
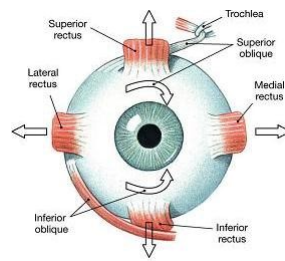
Figure 4.3: Extraocular muscles of the eye. Image from Google.

Our prototype only has 2 degrees of freedom (DOF) per eye, and hence the rotational oblique movements provided by the superior and inferior oblique muscles cannot be reproduced in our prototype. In these scenarios, the eyes of the prototype move to the new position in two steps by making two distinct horizontal and vertical movements.

Chapter 5

Development of a model of the Oculomotor System

This chapter describes the main contribution of the thesis, which is the development of an SNN that, by imitating structure requires no learning to control the robotic head presented in chapter 2. The inspiration for the system is based mostly on the saccade system of human vision (82). In the brain, saccade control structures are grouped into two regions for vertical and horizontal movement control, namely the vertical gaze center (riMLF) and the horizontal gaze center (PPRF), found in the pons region of the brainstem (82, 83, 84). We take inspiration from these structures to design our oculomotor spiking neural network model. The first part of the chapter will introduce these brain regions involved and then we present our spiking neural network model for the oculomotor system. Finally, we introduce reward based learning in the model for saccade gain adaptation.

5.1 Saccade Control: Neural Structures

The saccade control neurons are concentrated around two regions of the brainstem, the pontine paramedian reticulate formation (PPRF) and rostral interstitial nucleus of the medial longitudinal fasciculus (riMLF). The neurons in PPRF control horizontal saccades (84) and the neurons of riMLF control vertical saccades. These regions are called the horizontal and vertical gaze centers of the brain. The neurons identified in these regions generate a burst response depending on the input from the superior colliculus (SC).

The burst generation neurons identified in PPRF are the Long Lead Burst Neurons (LLBNs), Excitatory Burst Neurons (EBNs) and Inhibitory Burst Neurons (IBNs). The

response from SC triggers both the LLBN and the EBN, however only the LLBNs respond initially. Another class of neurons, omni-pause neurons (OPNs), control fixation and maintaining gaze given a target. The OPN neurons inhibit the EBNs and IBNs, thereby inhibiting the entire brust generation network and hence inhibiting movement of the eyes. Projections from the SC to the OPN, reduce the inhibiting effect of the OPN on the rest of the burst generation network. The combined effect of LLBN response and the reduction in OPN inhibition triggers an EBN response. The EBN response triggers the IBN response, which inhibits the contralateral burst neurons. The IBN response promotes conjugate movement of the eyes. The projections from the IBN to the OPN, reduce the OPN inhibition long enough for the eyes to complete the saccade. Finally, the EBNs project to the ipsilateral abducens nucleus and to interneurons which project to the contralateral oculomotor nucleus. The abducens nucleus and the oculomotor nucleus then send their tonic response to ipsilateral lateral rectus muscle and the contralateral medial rectus muscle respectively (83, 82, 4).

Although the neural structure described above is limited to conjugate horizontal eye movements, there are several neurons among the LLBNs and EBNs identified in the PPRF that respond only during vergence movements. Hence, the neurons in PPRF control both conjugate and vergence horizontal movements.

Similarly, in the riMLF, there mesencephalic vertical burst neurons, responsible for generating the vertical burst response based on SC input. The burst generation neurons from the riMLF project to the oculomotor nucleus and the trochlear nucleus, which in turn send their tonic response to the ipsilateral inferior rectus, superior rectus, inferior oblique and contralateral superior oblique (trochlear) respectively.

The control of neck movements during saccades involve the vestibular system (89). The vestibular system receives its inputs from both the SC (88) and the brainstem. We won't be discussing the details of the vestibular system in much further detail here. The vestibular system is assumed to have motor neurons that receive input from the SC and generate a motor response.

5.2   Replicating Retina structure in Camera input

The vision to build a neuro-inspired oculomotor controller would not be possible without replicating the foveated structure and the retinotopic organization preserved through the visual pathway (65). The foveated structure, as was described in Chapter 2, stems from the distribution of the photoreceptor cells in the retina. Hence the retinotopic organization, from the photoreceptors to the ganglion cells, helps localize the activity in the superior colliculus to a subset of neuron representing the region of the visual map containing the target.

In our model, we replicate foveated vision by dividing each frame from the camera into squares. Every frame is first resized to a square of side 720 pixels. This square image is then subsequently divided into multiple smaller squares concentrically, such that the size of the square keeps reducing as we move closer to the center of the image, our fovea. The artificial foveated structure in our model is represented in Figure 5.1. In this structure, we assume that there is no overlap between the pixels corresponding to different squares in this artificial fovea, though this assumption is not biologically accurate.

Since we do not model all the layers of the visual system and begin our model at the Superior Colliculus (SC), replicating the retinotopic organization is a simpler problem. We assume that the visual field representation at the superior colliculus maps exactly to the artificial foveated retinal representation imposed on each frame of the image. Based on this assumption, we assign a colliculus neuron to each square of the artificial retina, such that any activity within the square would trigger a response from that colliculus neuron.

The input from the superior colliculus to the oculomotor neurons provide both the amplitude and direction of the target. The neural response of the SC neurons needed to be scaled so that the collective response of the SC can accurately represent the different regions around the fovea. We model this by assigning different weights to the SC neurons depending on their position with respect to the fovea, using the pixel coordinates as the frame of reference. The weight of the projections from the SC neurons to the burst
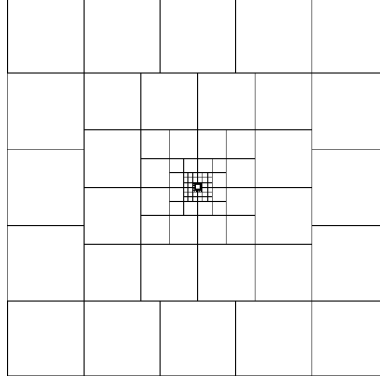
Figure 5.1: Receptive Field of superior colliculus neurons mapped to the image as seen by the retina. Each square in this image is mapped to a neuron in the superior colliculus. The neurons respond when there is any input within their receptive field.

generation networks was varied logarithmically around all sides of the fovea, we show the normalized weight distribution in Figure 5.2.
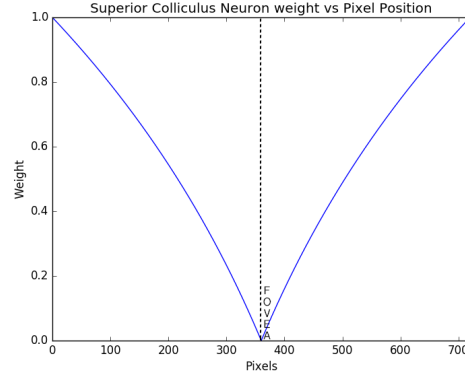
Figure 5.2: Variation of superior colliculus neuron weight with respect to its retinotopic pixel position. The same weight distribution is used for both horizontal and vertical distances, although we represent only one of the two in this figure.

The SC input is then sent to the horizontal and vertical oculomotor controller SNNs. Imitating the distinction in the brain regions controlling horizontal (PPRF) and vertical gaze (riMLF), in our model we send the inputs from the SC neurons that correspond to different parts of the visual field to the corresponding SNNs that control horizontal and vertical movements. For instance, SC neurons that map to the left half of the visual field would project to the horizontal oculomotor SNN, and specifically to neurons within this SNN that control movement towards the left.

For our primitive oculomotor system which can track one target, purely based on the

intensity difference between the target and the background, the assumptions we've made that are not biologically accurate do not make a significant difference. If additional layers were to be added to make the model biologically accurate, the function of this oculomotor model will still remain intact as long as the retinotopic organization is preserved through the layers. However, the assumption that the ganglion cell receptive fields and in turn superior colliculus receptive fields are square will need to change if we were to extend the system to include shape detection and similar higher order functions. Using a circular center-surround receptive field, as has been observed in the eye (21), would be ideal for these cases.

5.3 SNN for Horizontal Movement

We present the spiking neural network for oculomotor control of horizontal saccades in Figure 5.3.

In addition to the neurons identified in the PPRF, in our model, we've Ipsilateral Feedback Neurons (IFNs) and Tonic Neurons (TNs) and Motor Neurons (MNs).

The IFNs provide a local feedback within the burst generation circuit to inhibit the LLBN firing rate allowing for the eyes to move. The IFN inhibition is triggered when the EBNs generate their saccadic burst response, which helps in accurately encoding the target distance vector signal from the SC into a burst of action potentials (83).

The TNs and MNs are motor structures, corresponding to the neurons in the abducens and the oculomotor nuclei. The EBN response triggers the tonic response of TNs and then the evoked firing rate of MNs are translated into an equivalent servo position between 0 to 1023.

With horizontal movement, the added complexity of vergence or dis-conjugate movement exists. The most common scenario where dis-conjugate movement is observed is when the target is between the two eyes. In this case, the eyes need to move different amounts to focus on the target. This specific phenomenon is handled by the same regions of the brain (85), wherein the neurons take into consideration the input from both the eyes to generate an appropriate oculomotor response for both the eyes.
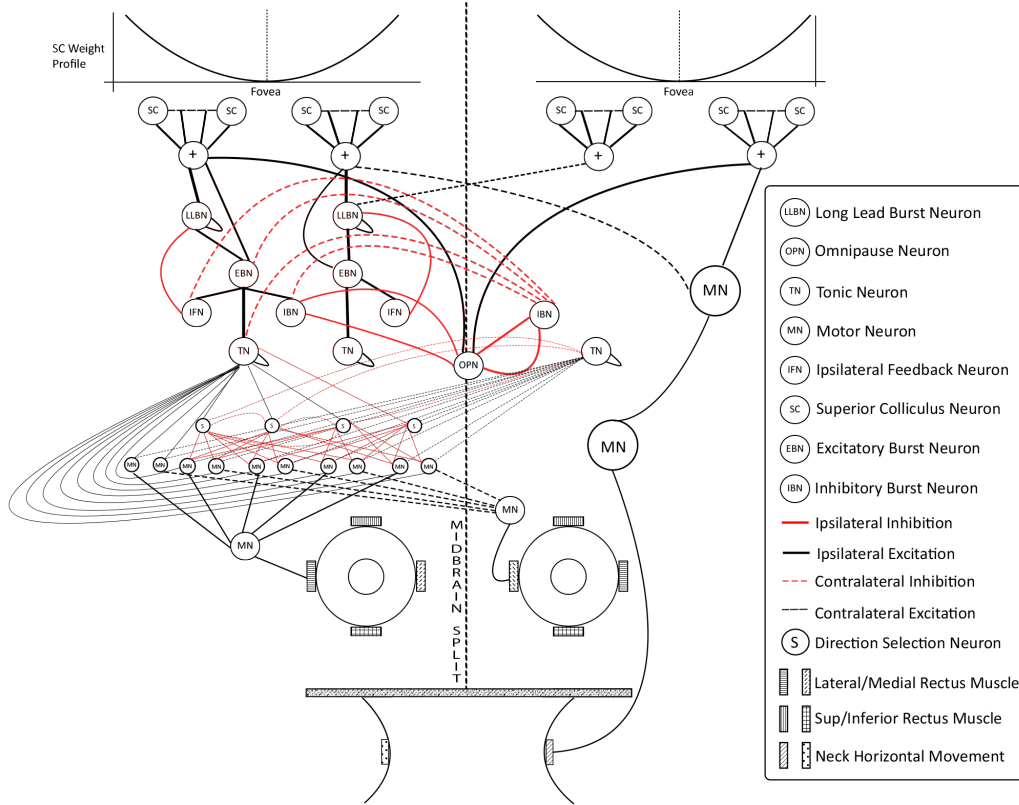
Figure 5.3: Oculomotor neurons found in the PPRF responsible control of horizontal movement of the eyes. The representation is for movement in a specific direction, especially focused on moving the eyes to the left and the neck to the right. The structure for left and right movement are symmetric and a similar network of neurons is present on the right half, which is omitted for clarity.

Vergence saccades are more complicated than conjugate saccades purely because of the change in direction of movement of the two eyes. In conjugate movements, due to the structure of the network, we can eliminate movement of the eyes in opposite direction by controlling them together. For instance, when the eyes need to move left, the neural network that generates the burst of spikes that control movement of the left eye towards the left, also controls the movement of the right eye towards the left. In addition, the IBNs that are active when the left eye moves left also inhibits the neural network that controls movement of the right eyes towards the right (83). In case of vergence movements, the dynamics of this networks needs to change, i.e. the eye movements are not coordinated.

We achieve this dual mode of operation for horizontal movement of the eyes by

introducing direction selective neurons (86). These neurons are labeled as S neurons in Figure 5.3. They determine the dominant stimulus between the conjugate and vergence inputs to generate the motor response.

5.4 SNN for Vertical Movement
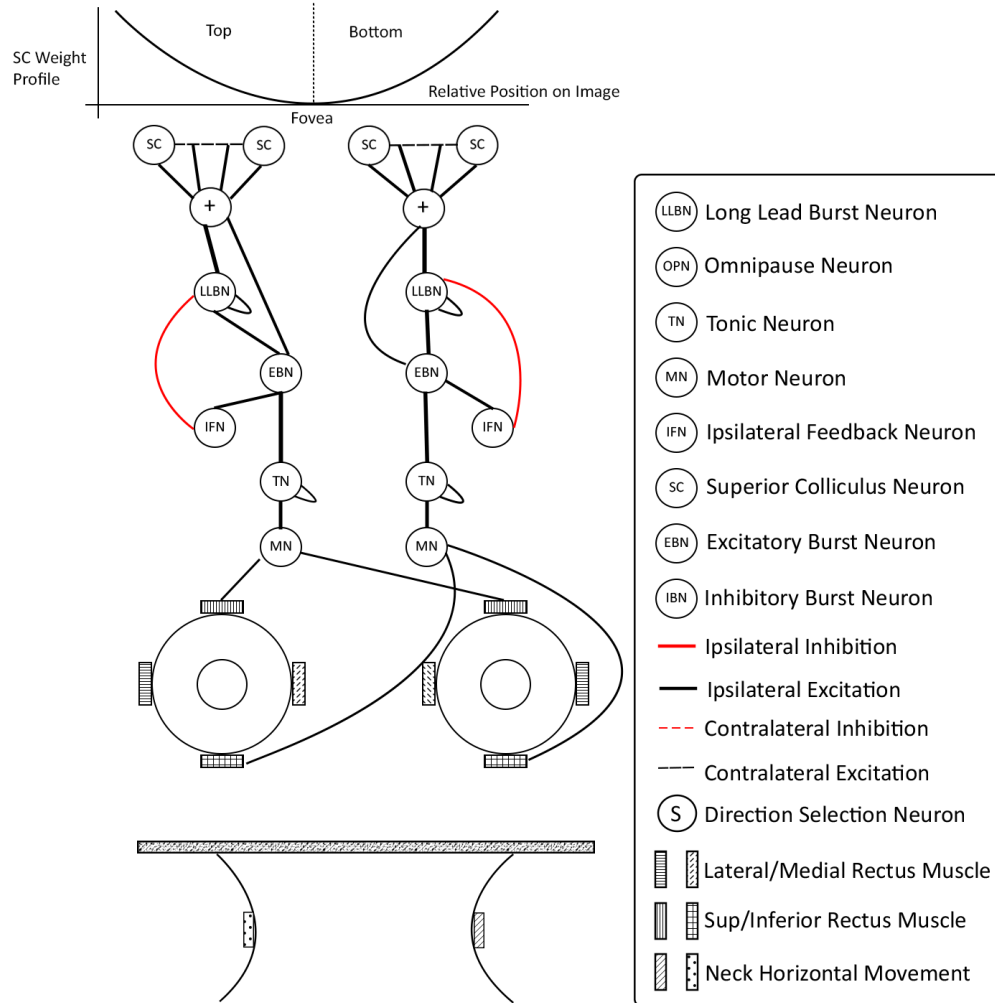
Figure 5.4: Vertical eye movement oculomotor network. The input SC neurons correspond to the neurons in the top half above the fovea and the bottom half above the fovea for both eyes. The input from the two eyes are used together to generate coordinated movement of both eyes upward or downward.

The vertical movement is much simpler than horizontal movement. For our prototype, we assume the eyes always move together, i.e. the vertical positions of both the eyes are always the same. Based on that assumption, the input to the vertical movement neural network is from the SC neurons that map to pixels that are in the top half of the image and the bottom half of the image. A weighted average of the vector input from both eyes are considered by the network to compute the effective eye position for the new target.

As with horizontal movement, the vertical eye movement also requires some bit of coordination. For certain inputs, the burst responses for upward and downward motion might be active at the same time. The burst response with the higher firing rate is chosen as dominant direction of movement and this dominant response is sent to the extra-ocular muscles. The neural network that generates the vertical movement burst response is shown in Figure 5.4.

Similar to horizontal movement, the firing rate based encoding is used to compute the servo position between 0 to 1023 which is then sent to the servo.

5.5   SNN for Neck Movement

The final part of the model is the neck movement. Movement of the neck extends the range of vision given the limited range of movement possible for the eyes within the orbital socket.

There is an intricate coordination between the vestibular and oculomotor system. The vestibular system has connections with the oculomotor system to signal the oculomotor system to initiate compensatory eye movements when the head moves (90, 91, 92). This is the vestibulo-ocular reflex movement of the eye that was discussed earlier.

The oculomotor system provides additional inputs to the vestibular system to move the neck, providing the signal that the eye movement was not sufficient to focus the target on the fovea. Physiologically, the delay in movement of the neck is because neck movement involves larger muscle activation.

In our prototype, we used the superior colliculus input as the main source of input for the neck movement. The vestibular system in the prototype does not have a burst generation circuit, they are instead integrating motor neurons. The SC input is integrated over time and only if the eyes cannot reach the target the neck movement is triggered. The delay in the neck movement is generated by the structure of the connections and the behavior of the leaky integrator neuron. The control of movement towards the right for the neck is also depicted in the Figure 5.3.

Since the neck movement is in all 4 directions, the weighted input from the SC neurons for neck movement is taken from all the SC neurons, representing left, right, top and bottom of the frame.

5.6   Biologically constrained Reward Based Learning

The model described imitates structures found in the brain and required no learning to function. The weights for the connections were taken from physiological studies and hence the model had reasonable performance even without learning.

In the oculomotor system, it is interesting to note that saccade gain adapts. The saccade amplitude (gain) is changed either by bottom-up visual error signals (94) or by top-down behavioral goal signals (93). To introduce learning, i.e. saccade adaptation, the visual error is introduced by moving the target when the saccade is initiated, forcing the eyes to adapt to the new target. Similarly, for behavioral goals, the target could be a character in an array of characters displayed on a screen. The position of the target character could be switched every trial at random, forcing the oculomotor system to adapt.

In our model, we introduced bottom-up, i.e. visual error based learning to observe the behavior of the system.

Traditionally, learning in neural networks is either supervised or unsupervised. Supervised learning requires training the network with a known set of inputs and expected responses from the network. Although supervised learning can be introduced in spiking neural networks, the oculomotor system is not a good candidate network for supervised

learning. The target trajectory is random and saccade adaptation to a known sequence of inputs is not useful. Unsupervised learning on the other hand does not rely on any known input - output relationships and the network is tasked with identifying patterns in the input and learning from any patterns that might be observed. Additionally, conventional approaches like gradient descent (back propagation) cannot be applied to spiking neural networks (SNNs) as well due to the asynchronous nature of inputs and parallel pathways in SNNs.

There are a few Hebbian learning algorithms for SNNs, the most common of these are either based on firing rate or the spike times. They are called rate based learning rules and spike time dependent plasticity (STDP) rules. In both these approaches, the weight changes Δw_{ij} depends only on the correlation between pre and post synaptic activity. Both these approaches are unsupervised learning approaches for SNNs.

Since we have an error signal from the visual system, a suitable middle ground for our system is reward based learning.

Reward based Sejnowski Learning Rule

Reward based learning relies on maximizing the reward that can be achieved in the network. Being a behavioral paradigm, the SNNs can learn based on a reward signal generated when the network performs as expected. In our case, we introduced reward based learning in the SNN. Every neuron in the network expects a certain reward and adapts to meet the reward target. The reward is maximal when the target is on the fovea, thus promoting the behavior of the network to bring the target onto the fovea. The reward signal profile is shown in Figure 5.5 Physiologically, the synapses receive the reward signal and have a memory of the previous reward signal, modulating the weight between a pair of neurons depending on the reward signal.

We used a global reward signal applied to all the neurons of the oculomotor system. However, the synaptic adaptation is local, i.e. the weight change depends not only on the reward signal but also on the pre-synaptic and post-synaptic neuron activities at the synapse. The synapse also has a memory of the pre-synaptic and post-synaptic spike timings.
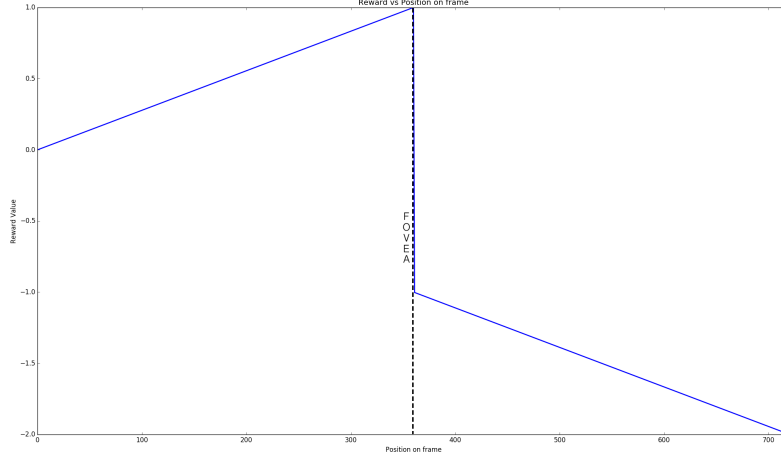
Figure 5.5: Reward variation with respect to the position of the target on the frame. The fovea is assumed to be at position = 360.

For every pair of pre-synaptic neuron j and post-synaptic neuron i, reward based hebbian learning is defined by the following set of equations,

$$\tau_e \frac{d}{dt} e_{ij} = -e_{ij} + H(pre_j, post_i)$$
$$\frac{d}{dt} w_{ij} = M.H(pre_j, post_i)e_{ij} \tag{5.1}$$
$$M(t) = R(t) - \langle R \rangle$$

where e_{ij} is the eligibility trace for the pair of neurons, w_{ij} is the weight of the synapse between the neurons, H is the hebbian learning term and $M(t)$ is the reward at time t. From these equations it can be observed that in addition to hebbian learning parameters such as pre- and post-synaptic activities, the weight changes also depend on a reward term (5).

For the hebbian learning term ($H(pre_j, post_i)$), we used the Sejnowski learning rule (114, 5). This rule relies on the activity of the pre and post synaptic neuron as well as the rate of spikes of these neurons over a short window. It is based on the idea that, firing rate of the neurons vary around their mean values $\langle v_i \rangle, \langle v_j \rangle$. The learning rule is represented in the following equation,

$$\frac{d}{dt} w_{ij} = \gamma \, (v_i - \langle v_i \rangle) \, (v_j - \langle v_j \rangle) \tag{5.2}$$

where γ is the learning rate.

Putting these two together, the reward based Sejnowski learning rule can be represented by the following equations,

$$\frac{d}{dt}w_{ij} = (R(t) - \langle R \rangle).H(pre_j, post_i).e_{ij}(t)$$

$$H(pre_j, post_i) = \gamma \ (v_i - \langle v_i \rangle) \ (v_j - \langle v_j \rangle) \qquad (5.3)$$

$$\tau_e \frac{d}{dt}e_{ij} = -e_{ij} + H(pre_j, post_i)$$

Chapter 6

Results

Our neuro-inspired oculomotor controller, used two approaches to design the SNN. The first approach by imitating the structures observed in the brain laid the base for the network upon which we introduced biologically constrained learning rules. In both the approaches, the oculomotor controller had good target tracking performance.

6.1   Methods

For all the experiments, we use an independent program (written in Python) to control the position of the laser target on the wall. The servo positions of the pan/tilt system that control the target position are recorded and converted to angle representations based on the initial calibration (refer Appendix).

The Oculomotor controller SNN (written in C++) is coordinated with the laser control program by means of a state file. When the oculomotor controller is initialized, the laser target is moved in defined sequences, depending on the experiment. The individual servo positions of the three pan/tilt systems of the robot prototype are recorded whenever the position of the eyes change (approximately every 22 ms). These positions are converted to angle representations based on the initial calibration values (refer Appendix). We compared these kinematics of the laser and the eye for accuracy measurements.

In all of the kinematics based results, the sign of the angles represent position of the target with respect to the origin. For horizontal movement, the negative and positive angles represent positions towards the left and right respectively. Similarly, for vertical movement, negative and positive values represent positions towards the bottom and top.

The effect of neck kinematics is added to the horizontal and vertical components of each eye. Since we allow head position changes, the eye positions are offset by the neck position changes. To factor this into our estimate for the eye gaze location, we add the neck kinematics response to the eye kinematics, allowing us to compare target position with respect to the gaze of the eyes.

For learning based experiments, we chose a repetitive pattern of target positions as the training input. The training pattern is repeated ten times, and the mean accuracy over each training sequence is used as a measure of behavioral convergence or learning.

6.2 Tracking accuracy of SNN imitating structure
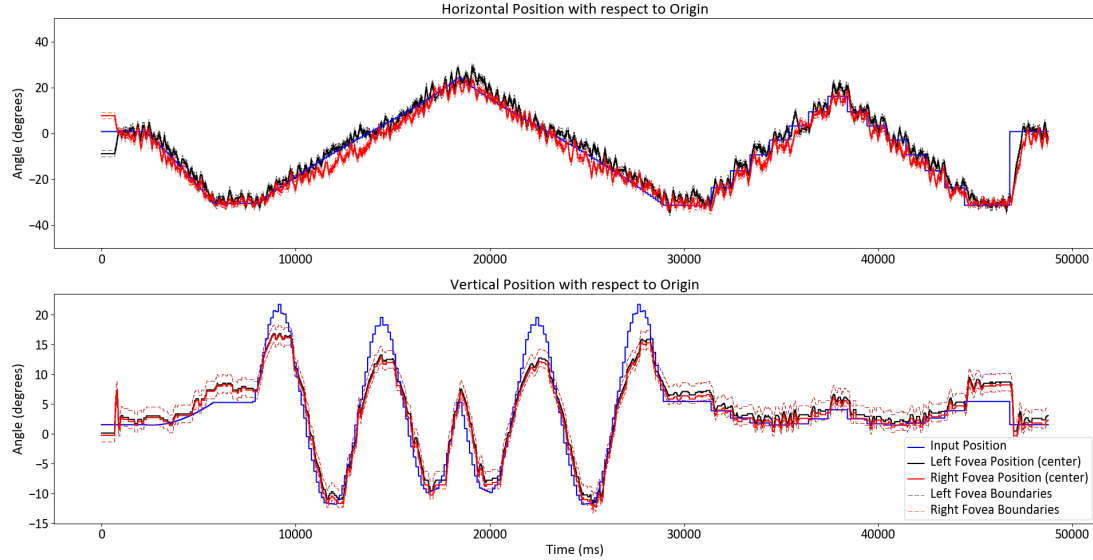
Figure 6.1: Kinematics of the eye with respect to the kinematics of the target. The target, shown in blue, is moved around through a sequence of positions on the wall demonstrating sudden changes in both horizontal and vertical directions. The eyes, shown in red and black, follow the target by making multiple saccade like movements. Top, shows the horizontal kinematics of the eye with respect to the target and bottom, shows the vertical kinematics with respect to the target.

In the implementation that relied only on imitating the structures found in the brain, we used weights adapted from literature and some other weights in the network were engineered. The mean relative error for the kinematics, averaged over both horizontal

and vertical direction of both the eyes and neck, was observed to be -0.685°. The kinematics of the prototype with respect to the kinematics of the laser target on the wall is as shown in Figure 6.1.

We observed an interesting phenomenon by imitating structure, micro-saccades. Although we did not design for them, the controller imitated micro-saccade like movement of the eyes, especially in the horizontal direction, when the target was stationary and the eyes were focused on the target. We attribute this behavior to the property of the controller which tries to focus the entire target within the bounds of the fovea. If the dimensions of the fovea are smaller than the target size on the frame, the controller constantly readjusts itself to attempt to fit the target within the fovea. This created an oscillatory behavior for the eyes once they reach the target. From Figure 6.1, we can observe the right (red) and left (black) eye traces oscillating around the input (blue) position.

Individually, the movement of the eyes and neck, were correlated with the neural activity in the oculomotor controller. For horizontal movement, its relation with the spiking of the SNN is shown in Figure 6.2. Similarly, for vertical movement, its relation to the spiking of the SNN is shown in Figure 6.3.
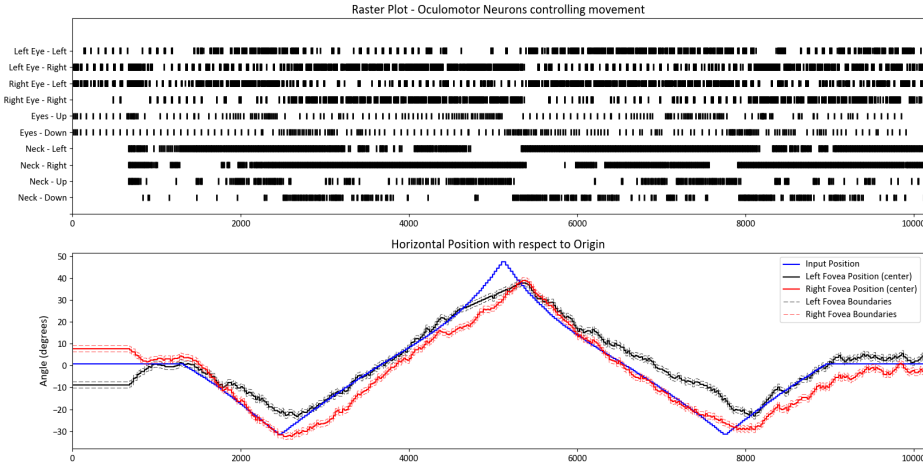
Figure 6.2: Horizontal Kinematics of the eyes influenced by the spike response of the oculomotor controller SNN.

From Figure 6.3, it can be observed that the vertical movement is delayed and when
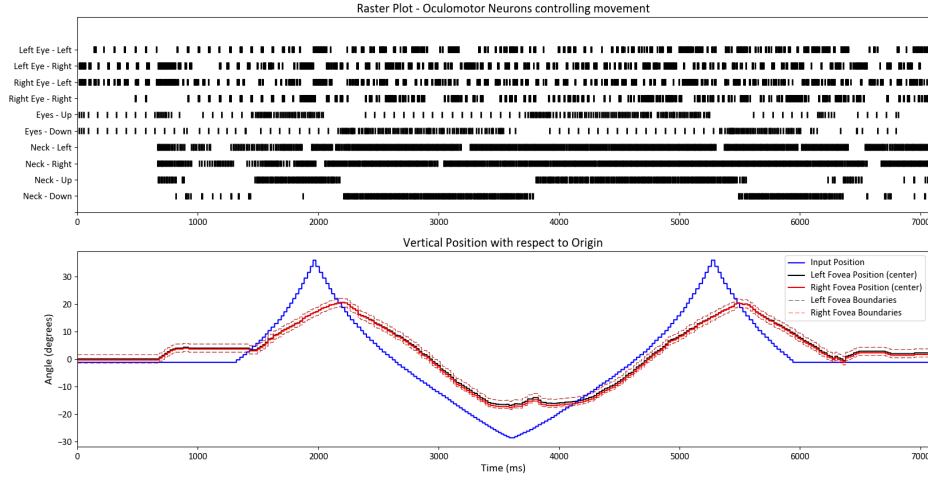
Figure 6.3: Vertical Kinematics of the eyes influenced by the spike response of the oculomotor controller SNN.

the target position changes rapidly in the vertical direction, the eyes cannot catch up with the target.

6.3 Behavioral Convergence with Reward-based Learning

When we introduced reward based learning into the SNN, the trained network had better target tracking kinematics. A noticeable improvement in tracking was observed for targets with rapidly growing vertical components. To quantify this, we presented a defined sequence of target positions to the controller with and without learning for a single trial. The kinematics of the eyes without and with learning is shown in Figure 6.4 and Figure 6.5.

Quantitatively, we compared the median relative error (R.E.) and root mean square error (RMSE) for horizontal and vertical kinematics of each eye in Table 6.1. From this comparison, we found that with learning the accuracy of eye kinematics improves, both in the relative error and root mean square error.
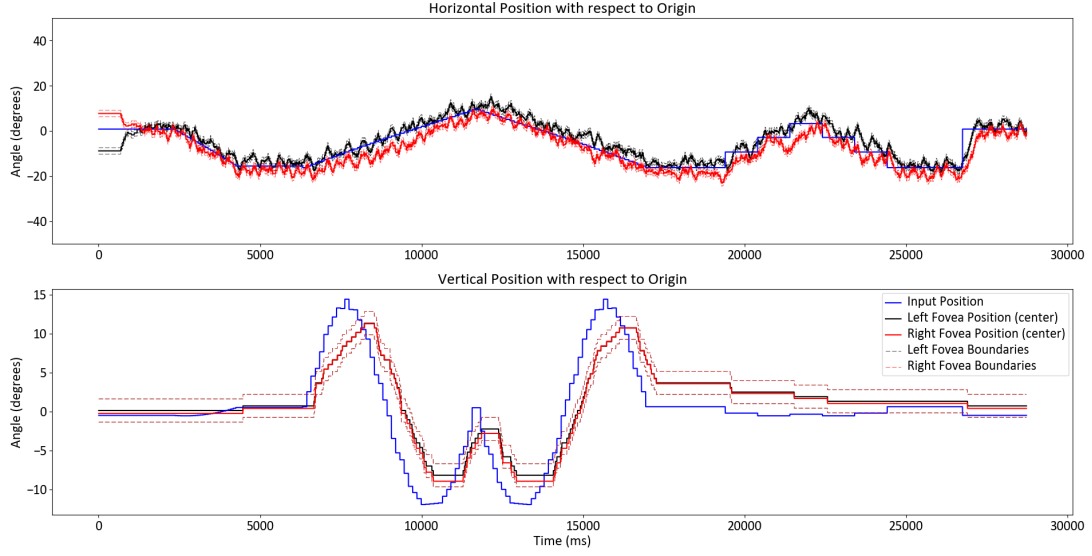
Figure 6.4: Kinematics of the eyes for a sequence of target positions without learning.
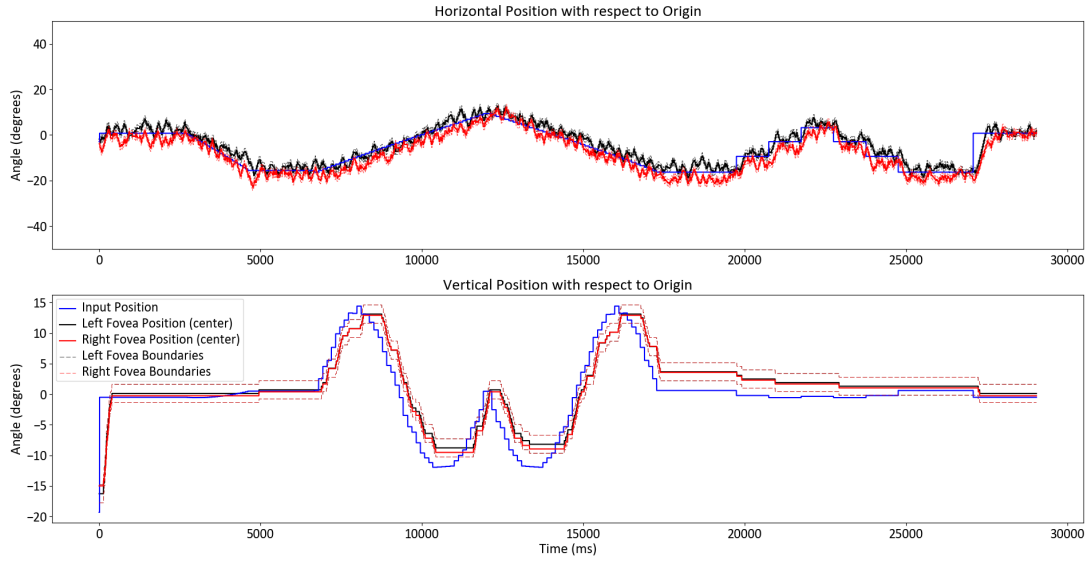
Figure 6.5: Kinematics of the eyes for a sequence of target positions with reward based learning.

In addition, we compared the effect of learning behaviorally by training the oculomotor controller with a sequence of inputs repeated ten times. The mean error is plotted for each iteration of training, repeated three times, as shown in Figure 6.6.

Factor	R.E. - NL	R.E. - L	RMSE - NL	RMSE - L
Left Eye - Hor.	-1.87°	-1.487°	3.55°	2.87°
Right Eye - Hor.	2.115°	2.049°	3.93°	3.44°
Left Eye - Ver.	-1.219°	-0.697°	3.14°	3.02°
Right Eye - Ver.	-0.823°	-0.421°	3.03°	2.95°

Table 6.1: Comparison of median relative error (R.E.) and root mean square error (RMSE) for eye kinematics with respect to the target with learning (L) and without learning(NL).
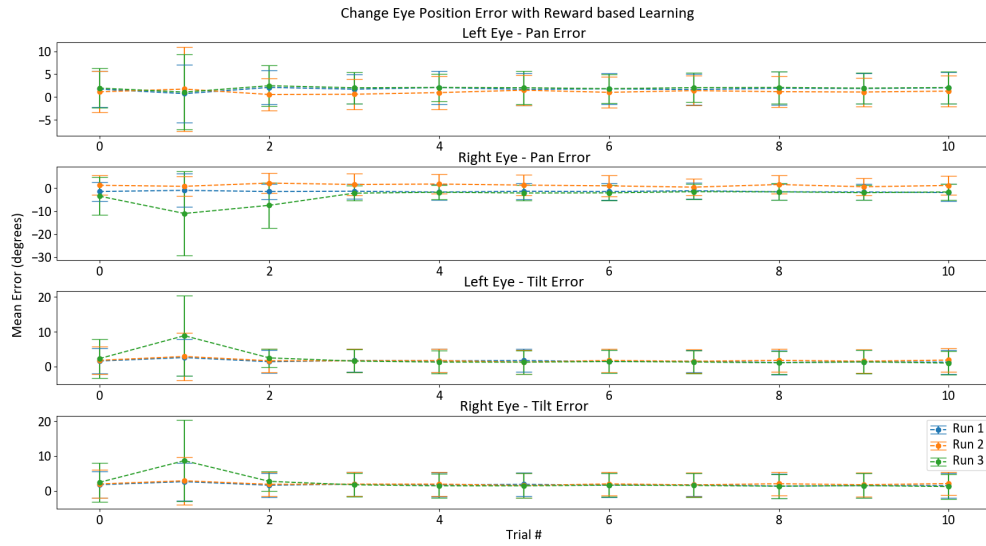
Figure 6.6: Mean error over a repetitive training sequence plotted for each iteration of training over 3 runs.

It was observed from Figure 6.6, that the behavior of the oculomotor controller converges as we train the controller over multiple iterations. The same response is observed over all three trials, although the errors observed during the initial iterations of training were not the same. These results suggested that the saccade adaptation which we aim to achieve through learning was successful, although there is still scope for improvement.

Chapter 7

Discussion

Our implementation of a neuro-inspired oculomotor controller for a robot prototype, is a first step towards building a more advanced neuro-inspired visual system. The body of existing knowledge around the oculomotor system simplified our efforts in building the oculomotor controller. However, many other parts of the visual system are still not clearly defined.

One of the issues we constantly faced during experiments was due to very high contrast sensitivity of the model. Random light sources in the corner of the visual field forced the eyes to move towards these targets. To imitate the behavior of the human visual system in these cases, i.e. adapting to sudden contrast changes, the introduction of center surround retinal receptive fields and maybe incorporating the neural layers of the retina into the model could prove worthwhile.

Another perspective on the same problem is considering the random light sources as additional targets. From a cognitive perspective, the saliency map representation in the frontal eye fields (FEF) could prove useful in determining the most salient target on the visual field.

Further experiments, including analyzing the behavior of the system to input more complicated than a single laser dot, such as a moving row and column of light with the intersection of the two being the target, could help us understand the limits of the current model. Using eye trackers to compare the behavior of the prototype with a human subject to the same input pattern could also provide interesting insights.

Future improvements, including object detection and tracking specific objects involves imitating the visual cortex in the model. The theories about the function of the different layers of the visual cortex have been proposed, but the exact mechanism in

which these functions are performed at a neuronal level is still unknown. Given the size of the visual cortex and the number of neurons, technology to simultaneously record the activity of all these neurons to study them is not available. Models at a population level, may help us understand the overall activity of the neurons but their usefulness in replicating their function using spiking neural networks will have to be evaluated.

In conclusion, this work introduces a new approach to design robot controllers, namely designing controllers using spiking neural networks inspired by structures in the brain. In addition to improving on the oculomotor system, building neuro-inspired controllers for motion planning, limb movements, gait replication in robots are just some ideas for further research.

Appendix A

Angle Calibration

The laser mounted on a pan/tilt system allowed us to move the target on the wall in 2 dimensions. The target position with respect to the origin is measured to determine the kinematics of the eyes as well as the kinematics of the target on the wall. Here, we assume the origin to be a point on a 2-D plane parallel to the plane of the eyes, such that it is at the intersection of the horizontal and vertical median between the two eyes at their starting position. The distance between the two parallel planes is taken to be 55 cm.

The calibration is two-fold for horizontal and vertical positions of the laser. The horizontal calibration is based on simple trigonometry. For different positions of the target on the wall, as shown in the Figure A.1, the angle from the origin β is measured by the formula $\beta = tan^{-1}(\frac{\alpha}{\delta})$. The distance $\delta = 55\ cm$, the distance from the wall to the plane of the eyes.
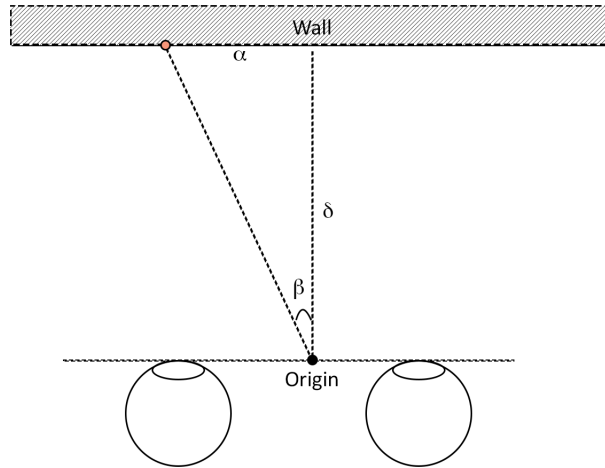
Figure A.1: Calibration Setup for Horizontal Calibration

The horizontal calibration measurements are tabulated in Table A.1. Based on the recorded data, we used linear regression analysis libraries to determine a higher order polynomial relation between angle and servo position, $\beta = f(pan)$. The same approach is used to determine a relationship between servo position and angle for all the servos.

Servo Position (pan)	X distance from Origin (α)	Angle (β)
50	24.8	24.15
65	12	12.24
75	7	7.21
84	0	0.0
101	-9.5	-9.75
112	-17.8	-17.84
122	-26	-25.18

Table A.1: Laser Horizontal Position Calibration (Pan)

A similar approach was used to estimate a relationship between servo positions of the left and right eyes and the angle their fovea made with the origin. The measured values are tabulated in Table A.2.

Servo Position (pan)	α (Left Eye)	β (Left Eye)	α (Right Eye)	β (Right Eye)
522	-12	-12.24	4.3	4.45
512	-9.5	-9.75	7	7.21
502	-6.3	-6.5	9.5	9.75
492	-4.0	-4.14	12	12.24
472	2.5	2.59	18	18.03
452	7.8	8.03	23.5	23.02

Table A.2: Eyes Horizontal Position Calibration (Pan)

The angle - distance relationship for pan seems to be almost linear. However, for tilt, the target position on the wall was more non-linear and varied with the pan position. This was due to the varying distance from the wall as the pan position changed, sometimes increasing the tilt angle. This stemmed from the height difference
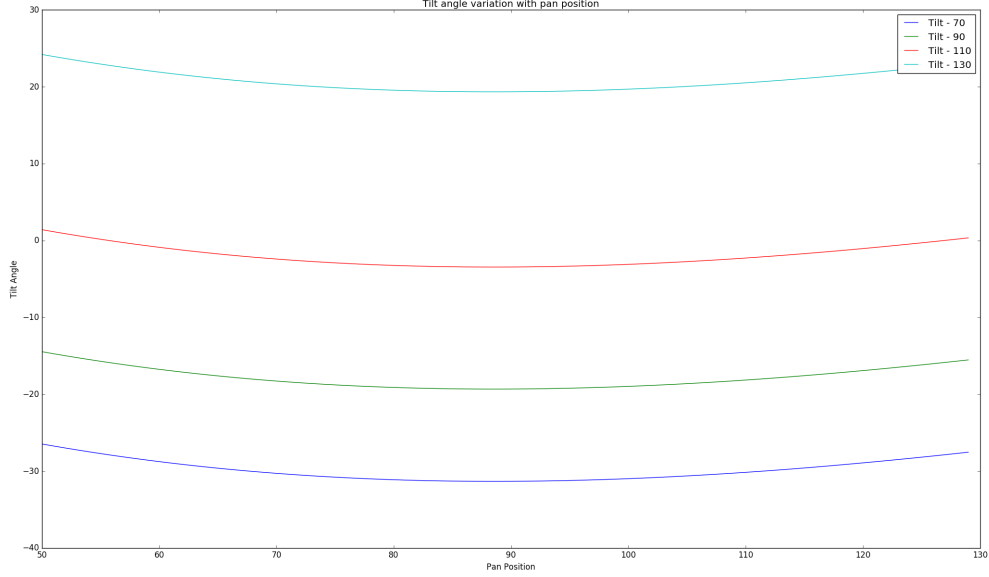
Figure A.2: Variation of laser tilt angle with pan servo position

between the laser source and the position of the Origin. The variation of tilt angle dependent on both pan and tilt position of the laser pan/tilt system is shown in Figure A.2. The measurements for tilt calibration of the eyes are tabulated in Table A.3.

Servo Position (pan)	α (Left Eye)	β (Left Eye)	α (Right Eye)	β (Right Eye)
462	16.2	14.98	15.8	14.59
502	4.8	3.52	4.6	3.31
512	1.4	0	1.4	0
522	-1.5	-3.00	-2.5	-4.03
562	-13	-14.59	-12.5	-14.11

Table A.3: Eyes Vertical Position Calibration (Tilt)

The non-linear calibration for the laser tilt servo yielded a relationship for angle β, dependent on both pan and tilt angles. We estimate the relationship by using a curve fitting algorithm upon the function,

$$\beta = f(x, y) = a + bx + cx^2 + dx^3 + ey + fy^2 + gy^3 \tag{A.1}$$

where x and y refer to the pan and tilt positions of the servo respectively. The values fed to the curve fitting algorithm are tabulated in Table A.4.

Pan	Tilt	α	β
84	114	0	0.0
50	114	6.5	6.12
110	114	1.2	1.19
70	130	19.6	19.27
60	130	23	21.78
100	130	18.7	18.45
60	90	-18.4	-17.73
100	90	-16.5	-16.4
80	70	-31.7	-29.78
70	70	-31.6	-29.41
110	70	-34	-30.55
120	70	-35.5	-30.45

Table A.4: Laser Vertical Position Calibration (Tilt)

Appendix B

Code

The Arbotix-M code to control the servos based on commands from the SNN is listed below.

```
/*
 * This code expects a message in the format: 512,512,512,512,512,512
 * This code requires a newline character to indicate the end of the data
 */


#include <ax12.h>            // ax12 servo control
#include <TextFinder.h>

TextFinder finder(Serial);

// Serial interface
#define BAUD_RATE 115200
#define NECK_PAN 1   // Dynamixel AX-12A servo IDs
#define NECK_TILT 2
#define LEFT_EYE_PAN 3
#define LEFT_EYE_TILT 4
#define RIGHT_EYE_PAN 5
#define RIGHT_EYE_TILT 6

const int NUMBER_OF_FIELDS = 6; // how many comma separated fields we expect
int fieldIndex = 0;             // the current field being received
int positions[6], newPositions[6];

void sendCurrentPosition() {
        Serial.print(positions[0]);
        Serial.print(',');
        Serial.print(positions[1]);
        Serial.print(',');
        Serial.print(positions[2]);
        Serial.print(',');
        Serial.print(positions[3]);
        Serial.print(',');
        Serial.print(positions[4]);
        Serial.print(',');
        Serial.print(positions[5]);
        Serial.println('\n');
}

bool positionsNotEqual() {
        return positions[0] != newPositions[0] || positions[1] != newPositions[1];
}

void setPosition() {
```

```
        int i;
        while(positionsNotEqual()) {
                for(i = 0; i < 2; i++) {
                        if(newPositions[i] > 400 && newPositions[i] < 700) {
                                if(positions[i] < newPositions[i])
                                        positions[i] += 1;
                                else if(positions[i] > newPositions[i])
                                        positions[i] -= 1;
                                SetPosition(i+1, positions[i]);
                        }
                }
                delay(1);
        }
        for(i = 2; i < 6; i++) {
                if(newPositions[i] > 400 && newPositions[i] < 700) {
                        SetPosition(i+1, newPositions[i]);
                        positions[i] = newPositions[i];
                }
        }
}


// Setup function
void setup() {
        // Set initial positions
        SetPosition(NECK_PAN, 512);
        SetPosition(NECK_TILT, 512);
        SetPosition(LEFT_EYE_PAN, 512);
        SetPosition(LEFT_EYE_TILT, 512);
        SetPosition(RIGHT_EYE_PAN, 512);
        SetPosition(RIGHT_EYE_TILT, 512);

        // Listen on serial connection for messages from the pc
        Serial.begin(BAUD_RATE);

        for(int i = 0; i < 6; i++)
                positions[i] = 512;
}


void loop()
{
        for(fieldIndex = 0; fieldIndex < NUMBER_OF_FIELDS; fieldIndex ++)
                newPositions[fieldIndex] = finder.getValue(); // get a numeric value
        setPosition();
        sendCurrentPosition();
        fieldIndex = 0;  // ready to start over
        delay(5);
}
```

The following code is part of the SNN that is the oculomotor controller. Here we illustrate the code for a generic Izhikevich neuron which we use and also a specific neuron, Long Lead Burst Neuron (LLBN), based on the Izhikevich model.

```
class IzhikevichNeuron {
public:
        IzhikevichParams params;
        vector<double> uValues;
        double u, v;

        vector<IzhikevichNeuron*> inhibitory;
```

```
vector<IzhikevichNeuron*> excitatory;

const string folderName = Constants::instance()−>outputDir;
string out_filename;
ofstream memb_out;


double v_max = 25;


double to_current(double membrane_potential) {
        if(membrane_potential == 25) { // Action potential
                return 1;
        }
        return 0;
}


IzhikevichNeuron(string filename) : out_filename(filename) {
        voltages.reserve(1000);
        uValues.reserve(1000);

        if(!memb_out.is_open()) {
                memb_out.open((folderName + out_filename).c_str(), ios::out);
        }
}


virtual double delta_v(double input_current) {
        double I = alter_current(input_current);
        if(I < 0)
                I = 0;
        return params.tau * (0.04 * pow(v, 2) + 5 * v + 140 − u + I);
}


vector<double> voltages;

IzhikevichNeuron(string filename, IzhikevichParams parameters)
        : out_filename(filename), params(parameters) {
        v = parameters.v_rest;
        u = parameters.b * v;
        voltages.reserve(1000);
        uValues.reserve(1000);

        if(!memb_out.is_open()) {
                memb_out.open((folderName + out_filename).c_str(), ios::out);
        }
}


double process(double input_current) {
        if(input_current < 0)
                input_current = 0;

        v += delta_v(input_current);
        u += params.tau * params.a * (params.b * v − u);

        if(voltages.size() == voltages.capacity() − 10)
                voltages.reserve(voltages.size() + 1000);

        if(uValues.size() == uValues.capacity() − 10)
                uValues.reserve(uValues.size() + 1000);
```

```cpp
                if(v > v_max) {
                        voltages.push_back(v_max);
                        v = params.c;
                        u += params.d;
                } else
                        voltages.push_back(v);
                uValues.push_back(u);
                memb_out << voltages.back() << endl;
                return voltages.back();
        }


        void reset() {
                v = params.v_rest;
                u = params.b * v;
        }


        void inhibitory_synapse(IzhikevichNeuron *nrn) {
                inhibitory.push_back(nrn);
        }


        void excitatory_synapse(IzhikevichNeuron *nrn) {
                excitatory.push_back(nrn);
        }


        virtual double alter_current(double input_current) {
                return input_current;
        }
};


class LLBN : public IzhikevichNeuron {
protected:
        double delta_v(double input_current) override {
                double I = alter_current(input_current);
                if(I < 0)
                        I = 0;
                return params.tau * (0.04 * pow(v, 2) + 4.1 * v + 108 - u + I);
        }
public:
        LLBN(string filename, IzhikevichNeuron *ifn_i) : IzhikevichNeuron(filename) {
                // Integrator params
                params.a=0.1;
                params.b=-0.075;
                params.c=-55;
                params.d= 6;
                params.v_rest=-60;
                params.tau = 1.0;
                v = params.v_rest;
                u = params.b*v;

                add_ifn_link(ifn_i);
        }


        // input_current = from sc (weighted)
        double alter_current(double input_current) override {
                double feedback_current = to_current(v);
                //IFN
                IzhikevichNeuron *ifn_i = inhibitory[0];
                int size = ifn_i->voltages.size();
```

```
double ifn_i_v = 0;
if ( size > 1) {
        ifn_i_v = ifn_i->voltages[size - 2];
}
return input_current * 125.0 * params.tau / 8
        - to_current(ifn_i_v) * 100.0 * params.tau / 8;
}

void add_ifn_link(IzhikevichNeuron *ifn_i) {
        this->inhibitory_synapse(ifn_i);
}
};
```

The Izhikevich neurons with different parameters are used in the SNN for different neuron types.

Appendix C

References

1. Andrew P. Wickens. (2014). A History of The Brain: From Stone Age surgery to modern neuroscience. New York: Psychology Press.

2. Giorgio Metta, Giulio Sandini, David Vernon, Lorenzo Natale, & Francesco Nori. (2008). The iCub humanoid robot: an open platform for research in embodied cognition. In Proceedings of the 8th Workshop on Performance Metrics for Intelligent Systems (PerMIS '08). ACM, New York, NY, USA, 50-56. doi:10.1145/1774674.1774683

3. Irving P. Herman. (2007). Physics of the Human Body. New York: Springer.

4. Eric R. Kandel, James H. Schwartz, Thomas M. Jessell, Steven A. Siegelbaum, A. J. Hudspeth, Sarah Mack. (2013). Principles of Neural Science. New York: McGraw-Hill.

5. Wulfram Gerstner, Werner M. Kistler, Richard Naud and Liam Paninski. (2014). Neuronal Dynamics: From single neurons to networks and models of cognition. Cambridge University Press.

6. Simon J. Thorpe, Karl R. Gegenfurtner, Michle Fabre-Thorpe, Heinrich H. Blthoff. (2001). Detection of animals in natural images using far peripheral vision. European Journal of Neuroscience, 14: 869876. doi:10.1046/j.0953-816x.2001.01717.x

7. Willi A. Ribi. (1981). The phenomenon of eye glow. Endeavour, Volume 5, Issue 1, 1981, Pages 2-8, ISSN 0160-9327, doi:10.1016/0160-9327(81)90072-7.

8. Chow, R. L., & Lang, R. A. (2001). Early eye development in vertebrates. Annual review of cell and developmental biology, 17(1), 255-296.

9. Schpf, V., Schlegl, T., Jakab, A., Kasprian, G., Woitek, R., Prayer, D., & Langs, G. (2014). The relationship between eye movement and vision develops before birth. Frontiers in Human Neuroscience, 8, 775. doi:10.3389/fnhum.2014.00775

10. Hosoya K, Tachikawa M. (2012). The inner blood-retinal barrier: molecular structure and transport biology. Adv Exp Med Biol.;763 85-104. PMID: 23397620.

11. Kazumichi Yoshida, Dai Watanabe, Hiroshi Ishikane, Masao Tachibana, Ira Pastan, Shigetada Nakanishi. (2001). A Key Role of Starburst Amacrine Cells in Originating Retinal Directional Selectivity and Optokinetic Eye Movement. Neuron, Volume 30, Issue 3, May 2001, Pages 771-780, ISSN 0896-6273, doi:10.1016/S0896-6273(01)00316-6.

12. Cook, P. B., & McReynolds, J. S. (1998). Lateral inhibition in the inner retina is important for spatial tuning of ganglion cells. Nature neuroscience, 1(8), 714-719. Chicago

13. M. Piccolino, J. Neyton, H. Gerschenfeld. (1981). Center-surround antagonistic organization in small-field luminosity horizontal cells of turtle retina. Journal of Neurophysiology, 45 (3) 363-375.

14. Bowmaker, J. K., & Dartnall, H. (1980). Visual pigments of rods and cones in a human retina. The Journal of physiology, 298(1), 501-511.

15. Curcio, C. A., Sloan, K. R., Kalina, R. E., & Hendrickson, A. E. (1990). Human photoreceptor topography. Journal of comparative neurology, 292(4), 497-523.

16. U Grunert, PR Martin. (1991). Rod bipolar cells in the macaque monkey retina: immunoreactivity and connectivity. Journal of Neuroscience, 11 (9) 2742-2758.

17. Calkins, D. J., Schein, S. J., Tsukamoto, Y., & Sterling, P. (1994). M and L cones in macaque fovea connect to midget ganglion cells by different numbers of excitatory synapses. Nature, 371(6492), 70-72.

18. Lisa J. Croner, Ehud Kaplan. (1995). Receptive fields of P and M ganglion cells across the primate retina, Vision Research, Volume 35, Issue 1, January 1995, Pages 7-24, ISSN 0042-6989, doi:10.1016/0042-6989(94)E0066-T.

19. Ev Famiglietti Jr., H Kolb. (1976). Structural basis for ON-and OFF-center responses in retinal ganglion cells. Science : 193-195.

20. Zeck, G. M., Xiao, Q. and Masland, R. H. (2005). The spatial filtering properties of local edge detectors and brisksustained retinal ganglion cells. European Journal of Neuroscience, 22: 20162026. doi:10.1111/j.1460-9568.2005.04390.x

21. Irvin, G. E., Casagrande, V. A., & Norton, T. T. (1993). Center/surround relationships of magnocellular, parvocellular, and koniocellular relay cells in primate lateral geniculate nucleus. Visual neuroscience, 10(02), 363-373. Chicag.

22. R. Nelson, E. V. Famiglietti, H. Kolb. (1978). Intracellular staining reveals different levels of stratification for on- and off-center ganglion cells in cat retina. Journal of Neurophysiology Mar 1978, 41 (2) 472-483.

23. EV Famiglietti Jr, H Kolb. (1976). Structural basis for ON-and OFF-center responses in retinal ganglion cells. Science Vol. 194, Issue 4261, pp. 193-195. doi:10.1126/science.959847

24. Dacey, D. M., & Petersen, M. R. (1992). Dendritic field size and morphology of midget and parasol ganglion cells of the human retina. Proceedings of the National Academy of sciences, 89(20), 9666-9670.

25. Itzhaki A, Perlman I. (1984). Light adaptation in luminosity horizontal cells in the turtle retina. Role of cellular coupling. Vision Res.;24(10):1119-26. PubMed, PMID: 6523733.

26. Wssle, H., Grunert, U., Chun, M.-N. and Boycott, B. B. (1995). The rod pathway of the macaque monkey retina: Identification of AII-amacrine cells with antibodies against calretinin. J. Comp. Neurol., 361: 537551. doi:10.1002/cne.903610315

27. Gouras, Peter. (1969). Antidromic responses of orthodromically identified ganglion cells in monkey retina. The Journal of Physiology, 204 doi: 10.1113/jphysiol.1969.sp008920.

28. Cleland BG, Levick WR. (1974). Properties of rarely encountered types of ganglion cells in the cat's retina and an overall classification. J Physiol.;240(2):457-92. PubMed PMID: 4420300; PubMed Central PMCID: PMC1331024.

29. Stewart A. Bloomfield, Ramon F. Dacheux. (2001). Rod Vision: Pathways and Processing in the Mammalian Retina. Progress in Retinal and Eye Research, Volume 20, Issue 3, May 2001, Pages 351-384, ISSN 1350-9462, doi:10.1016/S1350-9462(00)00031-8.

30. Ehud Kaplan, Barry B. Lee, Robert M. Shapley. (1990). Chapter 7 New views of primate retinal function, Progress in Retinal Research, Volume 9, Pages 273-336, ISSN 0278-4327, doi:10.1016/0278-4327(90)90009-7.

31. Lund JS, Lund RD, Hendrickson AE, Bunt AH, Fuchs AF. (1975). The origin of efferent pathways from the primary visual cortex, area 17, of the macaque monkey as shown by retrograde transport of horseradish peroxidase. J Comp Neurol.;164(3):287-303. PubMed PMID: 810501.

32. Edward M Callaway. (2004). Feedforward, feedback and inhibitory connections in primate visual cortex. Neural Networks, Volume 17, Issues 56, JuneJuly 2004, Pages 625-632, ISSN 0893-6080, doi:10.1016/j.neunet.2004.04.004.

33. Nealey, T. A., & Maunsell, J. H. (1994). Magnocellular and parvocellular contributions to the responses of neurons in macaque striate cortex. Journal of Neuroscience, 14(4), 2069-2079.

34. S A Engel, G H Glover, B A Wandell. (1997). Retinotopic organization in human visual cortex and the spatial precision of functional MRI. Cereb Cortex 1997; 7 (2): 181-192. doi: 10.1093/cercor/7.2.181

35. Dario L. Ringach. (2002). Spatial Structure and Symmetry of Simple-Cell Receptive Fields in Macaque Primary Visual Cortex. Journal of Neurophysiology Jul 2002, 88 (1) 455-463;

36. Ringach, D. L. (2004). Mapping receptive fields in primary visual cortex. The Journal of Physiology, 558: 717728. doi:10.1113/jphysiol.2004.065771

37. Cumming, B. G., & Parker, A. J. (1997). Responses of primary visual cortical neurons to binocular disparity without depth perception. Nature, 389(6648), 280-283.

38. Masson, G. S., Busettini, C., & Miles, F. A. (1997). Vergence eye movements in response to binocular disparity without depth perception. Nature, 389(6648), 283-286.

39. Geoffrey M Boynton, Jay Hegd. (2004). Visual Cortex: The Continuing Puzzle of Area V2. Current Biology, Volume 14, Issue 13, 13 July 2004, Pages R523-R524, ISSN 0960-9822, doi: 10.1016/j.cub.2004.06.044.

40. Lpez-Aranda, Manuel F. and Lpez-Tllez, Juan F. and Navarro-Lobato, Irene and Masmudi-Martn, Mariam and Gutirrez, Antonia and Khan, Zafar U. (2009). Role of Layer 6 of V2 Visual Cortex in Object-Recognition Memory. Science: Vol. 325, Issue 5936, pp. 87-89. doi: 10.1126/science.1170869

41. S. Shipp, J.D.G. Watson, R.S.J. Frackowiak, S. Zeri. (1995). Retinotopic Maps in Human Prestriate Visual Cortex: The Demarcation of Areas V2 and V3. NeuroImage, Volume 2, Issue 2, Part A, June 1995, Pages 125-132, ISSN 1053-8119, doi: 10.1006/nimg.1995.1015.

42. Lyon DC, Kaas JH. (2001). Connectional and architectonic evidence for dorsal and ventral V3, and dorsomedial area in marmoset monkeys. J Neurosci.;21(1):249-61. PubMed PMID: 11150342.

43. Oliver J Braddick, Justin M D O'Brien, John Wattam-Bell, Janette AtkinsonTom HartleyRobert Turner. (2016). Brain Areas Sensitive to Coherent Visual Motion. Perception: Vol 30, Issue 1, pp. 61 - 72. doi:10.1068/p3048

44. Robert Desimone, Stanley J. Schein, Jeffrey Moran, Leslie G. Ungerleider. (1985). Contour, color and shape analysis beyond the striate cortex, Vision Research, Volume 25, Issue 3, 1985, Pages 441-452, ISSN 0042-6989, doi: 10.1016/0042-6989(85)90069-0.

45. Luck, Steven J., Leonardo Chelazzi, Steven A. Hillyard, and Robert Desimone. (1997). Neural mechanisms of spatial selective attention in areas V1, V2, and V4 of macaque visual cortex. J. Neurophysiol. 77: 2442.

46. JD Schall, A Morel, DJ King, J Bullier. (1995). Topography of visual cortex connections with frontal eye field in macaque: convergence and segregation of processing streams. Journal of Neuroscience 1 June 1995, 15 (6) 4464-4487

47. Jennifer M. Groh, Richard T. Born, William T. Newsome. (1997). How Is a Sensory Map Read Out? Effects of Microstimulation in Visual Area MT on Saccades and Smooth Pursuit Eye Movements. Journal of Neuroscience 1 June 1997, 17 (11) 4312-4330

48. Vincent P. Ferrera, Stephen G. Lisberger. (1997). Neuronal Responses in Visual Areas MT and MST During Smooth Pursuit Target Selection. Journal of Neurophysiology Sep 1997, 78 (3) 1433-1446.

49. Velia Cardin, Andrew T. Smith. (2011). Sensitivity of human visual cortical area V6 to stereoscopic depth gradients associated with self-motion. Journal of Neurophysiology Sep 2011, 106 (3) 1240-1249; DOI: 10.1152/jn.01120.2010

50. Andreas Kleinschmidt, Kai V. Thilo, Christian Bchel, Michael A. Gresty, Adolfo M. Bronstein, Richard S.J. Frackowiak. (2002). Neural Correlates of Visual-Motion Perception as Object- or Self-motion. NeuroImage, Volume 16, Issue 4, August 2002, Pages 873-882, ISSN 1053-8119, doi: 10.1006/nimg.2002.1181.

51. S. Pitzalis, M.I. Sereno, G. Committeri, P. Fattori, G. Galati, F. Patria, C. Galletti. (2010). Human V6: The Medial Motion Area. Cereb Cortex 2010; 20 (2): 411-424. doi: 10.1093/cercor/bhp112

52. Bizzi, E.. (1968). Discharge of frontal eye field neurons during saccadic and following eye movements in unanesthetized monkeys. Exp Brain Res 6: 69. doi:10.1007/BF00235447

53. Martha G. MacAvoy, Jacqueline P. Gottlieb, Charles J. Bruce. (1991). Smooth-Pursuit Eye Movement Representation in the Primate Frontal Eye Field. Cereb Cortex; 1 (1): 95-102. doi: 10.1093/cercor/1.1.95

54. Petit, L., Clark, V. P., Ingeholm, J., & Haxby, J. V. (1997). Dissociation of saccade-related and pursuit-related activation in human frontal eye fields as revealed by fMRI. Journal of Neurophysiology, 77(6), 3386-3390.

55. Marrocco, R. T. (1978). Saccades induced by stimulation of the frontal eye fields: interaction with voluntary and reflexive eye movements. Brain research, 146(1), 23-34.

56. Thompson, K. G., & Bichot, N. P. (2005). A visual salience map in the primate frontal eye field. Progress in brain research, 147, 249-262.

57. Thompson, K. G., Bichot, N. P., & Schall, J. D. (1997). Dissociation of visual discrimination from saccade programming in macaque frontal eye field. Journal of neurophysiology, 77(2), 1046-1050.

58. Schnyder, H., Reisine, H., Hepp, K., & Henn, V. (1985). Frontal eye field projection to the paramedian pontine reticular formation traced with wheat germ agglutinin in the monkey. Brain research, 329(1), 151-160.

59. Sommer, M. A., & Wurtz, R. H. (2000). Composition and topographic organization of signals sent from the frontal eye field to the superior colliculus. Journal of Neurophysiology, 83(4), 1979-2001.

60. Rivaud, S., Mri, R. M., Gaymard, B., Vermersch, A. I., & Pierrot-Deseilligny, C. (1994). Eye movement disorders after frontal eye field lesions in humans. Experimental Brain Research, 102(1), 110-120.

61. Keating, E. G. (1991). Frontal eye field lesions impair predictive and visually-guided pursuit eye movements. Experimental Brain Research, 86(2), 311-323.

62. Schall, J. D. (2002). The neural selection and control of saccades by the frontal eye field. Philosophical Transactions of the Royal Society of London B: Biological Sciences, 357(1424), 1073-1082.

63. Jay, M. F., & Sparks, D. L. (1987). Sensorimotor integration in the primate superior colliculus. I. Motor convergence. Journal of neurophysiology, 57(1), 22-34.

64. Dorris, M. C., Pare, M., & Munoz, D. P. (1997). Neuronal activity in monkey superior colliculus related to the initiation of saccadic eye movements. Journal of Neuroscience, 17(21), 8566-8579.

65. Sparks, D. L., & Gandhi, N. J. (2003). Single cell signals: an oculomotor perspective. Progress in brain research, 142, 35-53.

66. Munoz, D. P., & Wurtz, R. H. (1992). Role of the rostral superior colliculus in active visual fixation and execution of express saccades. Journal of Neurophysiology, 67(4), 1000-1002.

67. Hafed, Z. M., Goffart, L., & Krauzlis, R. J. (2009). A neural mechanism for microsaccade generation in the primate superior colliculus. science, 323(5916), 940-943.

68. Bergeron, A., & Guitton, D. (2000). Fixation neurons in the superior colliculus encode distance between current and desired gaze positions. Nature neuroscience, 3(9), 932-939.

69. Orban de Xivry, J. J., & Lefevre, P. (2007). Saccades and pursuit: two outcomes of a single sensorimotor process. The Journal of Physiology, 584(1), 11-23.

70. Purves D, Augustine GJ, Fitzpatrick D, et al., editors. Neuroscience. 2nd edition. Sunderland (MA): Sinauer Associates; (2001). Types of Eye Movements and Their Functions. Available from: https://www.ncbi.nlm.nih.gov/books/NBK10991/

71. Martinez-Conde, S., Macknik, S. L., Troncoso, X. G., & Hubel, D. H. (2009). Microsaccades: a neurophysiological analysis. Trends in neurosciences, 32(9), 463-475.

72. Peterson, M. S., Kramer, A. F., & Irwin, D. E. (2004). Covert shifts of attention precede involuntary eye movements. Attention, Perception, & Psychophysics, 66(3), 398-405.

73. Fox, P. T., Fox, J. M., Raichle, M. E., & Burde, R. M. (1985). The role of cerebral cortex in the generation of voluntary saccades: a positron emission tomographic study. Journal of Neurophysiology, 54(2), 348-369.

74. Doyle, M., & Walker, R. (2001). Curved saccade trajectories: Voluntary and reflexive saccades curve away from irrelevant distractors. Experimental Brain Research, 139(3), 333-344.

75. Ross, S. M., & Ross, L. E. (1981). Saccade latency and warning signals: effects of auditory and visual stimulus onset and offset. Attention, Perception, & Psychophysics, 29(5), 429-437.

76. McPeek, R. M., Skavenski, A. A., & Nakayama, K. (2000). Concurrent processing of saccades in visual search. Vision research, 40(18), 2499-2516.

77. Barnes, G. R. (2008). Cognitive processes involved in smooth pursuit eye movements. Brain and cognition, 68(3), 309-326.

78. Barnes, G. R., & Asselman, P. T. (1991). The mechanism of prediction in human smooth pursuit eye movements. The Journal of physiology, 439, 439.

79. Priebe, N. J., & Lisberger, S. G. (2004). Estimating target speed from the population response in visual area MT. Journal of Neuroscience, 24(8), 1907-1916.

80. Keller, E., & Johnsen, S. S. (1990). Velocity prediction in corrective saccades during smooth-pursuit eye movements in monkey. Experimental Brain Research, 80(3), 525-531.

81. Tabareau, N., Bennequin, D., Berthoz, A., Slotine, J. J., & Girard, B. (2007). Geometry of the superior colliculus mapping and efficient oculomotor computation. Biological Cybernetics, 97(4), 279-292.

82. Sparks, D. L. (2002). The brainstem control of saccadic eye movements. Nature Reviews Neuroscience, 3(12), 952-964.

83. Scudder, C. A. (1988). A new local feedback model of the saccadic burst generator. Journal of Neurophysiology, 59(5), 1455-1475.

84. Scudder, C. A., Kaneko, C. R., & Fuchs, A. F. (2002). The brainstem burst generator for saccadic eye movements: A modern synthesis. Experimental brain research, 142(4), 439-462.

85. Van Horn, M. R., & Cullen, K. E. (2008). Dynamic coding of vertical facilitated vergence by premotor saccadic burst neurons. Journal of neurophysiology, 100(4), 1967-1982.

86. Ohtsuka, K., & Noda, H. (1990). Direction-selective saccadic-burst neurons in the fastigial oculomotor region of the macaque. Experimental brain research, 81(3), 659-662.

87. Wang, S. F., & Spencer, R. F. (1996). Spatial organization of premotor neurons related to vertical upward and downward saccadic eye movements in the rostral interstitial nucleus of the medial longitudinal fasciculus (riMLF) in the cat. Journal of Comparative Neurology, 366(1), 163-180.

88. Corneil, B. D., Olivier, E., & Munoz, D. P. (2002). Neck muscle responses to stimulation of monkey superior colliculus. II. Gaze shift initiation and volitional head movements. Journal of Neurophysiology, 88(4), 2000-2018.

89. Cullen, K. E., & Roy, J. E. (2004). Signal processing in the vestibular system during active versus passive head movements. Journal of neurophysiology, 91(5), 1919-1933.

90. Cullen, K. E., & McCREA, R. A. (1993). Firing behavior of brain stem neurons during voluntary cancellation of the horizontal vestibuloocular reflex. I. Secondary vestibular neurons. Journal of neurophysiology, 70(2), 828-843.

91. McCrea, R. A., Strassman, A., May, E., & Highstein, S. M. (1987). Anatomical and physiological characteristics of vestibular neurons mediating the horizontal vestibuloocular reflex of the squirrel monkey. Journal of Comparative Neurology, 264(4), 547-570.

92. Scudder, C. A., & Fuchs, A. F. (1992). Physiological and behavioral identification of vestibular nucleus neurons mediating the horizontal vestibuloocular reflex in trained rhesus monkeys. Journal of neurophysiology, 68(1), 244-264.

93. Schtz, A. C., Kerzel, D., & Souto, D. (2014). Saccadic adaptation induced by a perceptual task. Journal of vision, 14(5), 4-4.

94. Wallman, J., & Fuchs, A. F. (1998). Saccadic gain modification: visual error drives motor adaptation. Journal of neurophysiology, 80(5), 2405-2416.

95. Raichle, M. E., & Mintun, M. A. (2006). Brain work and brain imaging. Annu. Rev. Neurosci., 29, 449-476.

96. Berdondini, L., Imfeld, K., Maccione, A., Tedesco, M., Neukom, S., Koudelka-Hep, M., & Martinoia, S. (2009). Active pixel sensor array for high spatio-temporal resolution electrophysiological recordings from single cell to large scale neuronal networks. Lab on a Chip, 9(18), 2644-2651.

97. Garcia, E., Jimenez, M. A., De Santos, P. G., & Armada, M. (2007). The evolution of robotics research. IEEE Robotics & Automation Magazine, 14(1), 90-103.

98. Velsquez, J. D. (1998, July). When robots weep: emotional memories and decision-making. In AAAI/IAAI (pp. 70-75).

99. Brooks, R. A., Breazeal, C., Marjanovi, M., Scassellati, B., & Williamson, M. M. (1999). The Cog project: Building a humanoid robot. In Computation for metaphors, analogy, and agents (pp. 52-87). Springer Berlin Heidelberg.

100. Degallier, S., Righetti, L., Natale, L., Nori, F., Metta, G., & Ijspeert, A. (2008, October). A modular bio-inspired architecture for movement generation for the infant-like robot

iCub. In Biomedical Robotics and Biomechatronics, 2008. BioRob 2008. 2nd IEEE RAS & EMBS International Conference on (pp. 795-800). IEEE.

101. Kormushev, P., Calinon, S., Saegusa, R., & Metta, G. (2010, December). Learning the skill of archery by a humanoid robot iCub. In Humanoid Robots (Humanoids), 2010 10th IEEE-RAS International Conference on (pp. 417-423). IEEE.

102. Rosenblatt, F. (1958). The perceptron: A probabilistic model for information storage and organization in the brain. Psychological review, 65(6), 386.

103. Hopfield, J. J. (1984). Neurons with graded response have collective computational properties like those of two-state neurons. Proceedings of the national academy of sciences, 81(10), 3088-3092.

104. Hinton, G. E., Sejnowski, T. J., & Ackley, D. H. (1984). Boltzmann machines: Constraint satisfaction networks that learn. Pittsburgh, PA: Carnegie-Mellon University, Department of Computer Science.

105. Funahashi, K. I. (1989). On the approximate realization of continuous mappings by neural networks. Neural networks, 2(3), 183-192.

106. Schmidhuber, J. (2015). Deep learning in neural networks: An overview. Neural networks, 61, 85-117.

107. Mainen, Z. F., & Sejnowski, T. J. (1995). Reliability of spike timing in neocortical neurons. Science, 268(5216), 1503.

108. Mohemmed, A., Schliebs, S., Matsuda, S., & Kasabov, N. (2012). Span: Spike pattern association neuron for learning spatio-temporal spike patterns. International Journal of Neural Systems, 22(04), 1250012.

109. Meissirel, C., Wikler, K. C., Chalupa, L. M., & Rakic, P. (1997). Early divergence of magnocellular and parvocellular functional subsystems in the embryonic primate visual system. Proceedings of the National Academy of Sciences, 94(11), 5900-5905.

110. Thomson, A. M. (2010). Neocortical layer 6, a review. Frontiers in neuroanatomy, 4(13).

111. Cui, D. M., Yan, Y. J., & Lynch, J. C. (2003). Pursuit subregion of the frontal eye field projects to the caudate nucleus in monkeys. Journal of neurophysiology, 89(5), 2678-2684.

112. Sparks, D. L., & Gandhi, N. J. (2003). Single cell signals: an oculomotor perspective. Progress in brain research, 142, 35-53.

113. Lisberger, S. G. (2010). Visual guidance of smooth-pursuit eye movements: sensation, action, and what happens in between. Neuron, 66(4), 477-491.

114. Sejnowski, T. J. (1977). Storing covariance with nonlinearly interacting neurons. Journal of mathematical biology, 4(4), 303-321.